The expression of each gene was normalized with that of *18s* rRNA.

ELISA

ELISA for adiponectin and TNF-α was performed using commercially available kits (R&D systems, Inc., Minneapolis, MN, USA) in accordance with the manufacturer's instructions.

Statistical analysis

Statistical analysis was performed with one-way ANOVA and Fisher's test if appropriate. Data are shown as mean±S.E.M. $P<0{\cdot}05$ was considered to be statistically significant.

Results

Hemodynamic and metabolic parameters

Body weight was significantly increased in the HFD group compared with the control group at the end of the experiment. However, there was no significant difference between the HFD and BPS groups (Table 1). SBP was significantly increased in the HFD group compared with the control group. BPS significantly reduced SBP, but SBP in the BPS group was still significantly higher than that in control group (Table 1). HR was significantly increased in the HFD group compared with the control group. BPS reduced HR, but the difference was not statistically significant (Table 1).

After 16 h of fasting, lipid profile and glucose and insulin levels were determined. Total cholesterol and triglyceride were significantly increased by the HFD (Table 2). BPS treatment modestly decreased total cholesterol and triglyceride levels. However, the differences were not statistically significant. Fasting insulin and glucose levels were elevated in the HFD group.

BPS improved GTT and ITT

At the end of experiment, GTTs and ITTs were performed. The HFD group developed glucose intolerance (Fig. 1A) and insulin resistance (Fig. 1C). Treatment of mice with BPS significantly improved glucose tolerance and insulin action (Fig. 1A and C). Interestingly, the basal glucose level was significantly lower in the BPS group compared with the HFD group after 6 h of fasting, which was not observed after 16 h of fasting (Table 2). Area under the curves (AUC) also showed improvement of glucose metabolism by BPS treatment (Fig. 1B and D).

Table 1 BW, SBP, and HR

	BW (g)	**SBP** (mmHg)	**HR** (b.p.m.)
Control ($n=5$)	26·9±0·5	97±3	448±31
HFD ($n=10$)	43·4±1·1†	114±2†	532±15†
HFD+BPS ($n=10$)	43·9±0·9†	106±2*,‡	496±15

HFD, high-fat diet; BPS, beraprost sodium; BW, body weight; SBP, systolic blood pressure; HR, heart rate. $^{*}P<0{\cdot}05$, $^{\dagger}P<0{\cdot}01$ vs control. $^{\ddagger}P<0{\cdot}05$ vs HFD group.

Table 2 Fasting serum chemistry of control, HFD-, and BPS-treated mice

	TC (mg/ml)	**TG** (mg/ml)	**Insulin** (ng/ml)	**Glucose** (mg/ml)
Control ($n=5$)	55±4	66±12	0·16±0·05	59·6±2·6
HFD ($n=10$)	209±9†	94±9*	3·75±0·51†	142·4±7·3†
HFD+BPS ($n=10$)	182±14†	74±6	4·12±0·90†	132·8±6·2†

HFD, high-fat diet; BPS, beraprost sodium; TC, total cholesterol; TG, triglyceride. $^{*}P<0{\cdot}05$ and $^{\dagger}P<0{\cdot}01$ vs control.

BPS reduced adipocyte size

Histological analysis of epididymal WAT showed that the adipocyte size was increased in the HFD group compared with the control group (Fig. 2A and B). Treatment with BPS reduced adipocyte size (Fig. 2C). Statistical analysis confirmed that BPS significantly reduced adipocyte size (Fig. 2D). These data suggest that BPS enhanced adipocyte differentiation. We therefore examined expression of genes related to adipocyte differentiation. *Pparγ* was significantly suppressed by the HFD, which was reversed by BPS (Fig. 3A). The upregulation of *Pparγ* by BPS showed a borderline significance ($P=0{\cdot}06$) when three groups were considered. However, the difference between the HFD and BPS groups was statistically significant if only the HFD groups were compared ($P=0{\cdot}02$). We failed to see a significant effect of BPS treatment on the expression of C/EBPα (Fig. 3B) or adiponectin (Fig. 3C). Although adiponectin mRNA levels were not changed in the three groups, serum adiponectin levels were mildly decreased in the HFD group and BPS groups (Fig. 3D). However, the difference in serum adiponectin levels between the three groups was not statistically significant.

BPS reduced inflammatory changes in WAT in HFD-fed mice

Chronic inflammation in WAT is a common feature of obesity. Therefore, we examined the infiltration of macrophages into adipose tissue. The number of MAC3-positive macrophage aggregation surrounding adipocytes, often referred to as a crown-like structure (CLS) in WAT (Weisberg *et al.* 2003, Xu *et al.* 2003), was significantly increased in the HFD group compared with the control group (Fig. 2E and F; arrowheads). In the control group (Fig. 2E), almost no CLS was observed in WAT. Treatment with BPS significantly decreased the number of CLSs in WAT (Fig. 2G and H).

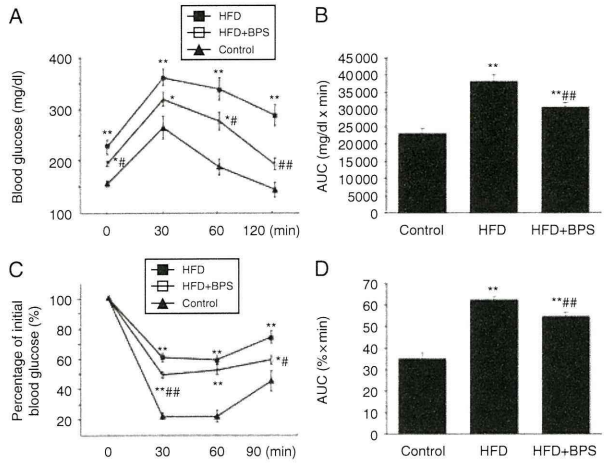

Figure 1 BPS ameliorated HFD-induced insulin resistance. (A) The control group (black triangle) was fed a normal chow and the HFD (black box) and BPS groups (white box) were fed a HFD for 12 weeks. Mice were i.p. injected with 1 g/kg glucose and blood glucose levels were measured. (C) Mice were i.p. injected with 0·5 U/kg insulin and blood glucose levels were measured. (B and D) AUC were calculated. Control group $n=5$, HFD group and BPS group $n=10$. $^{*}P<0{\cdot}05$ and $^{**}P<0{\cdot}01$ vs control. $^{\#}P<0{\cdot}05$ vs HFD group, $^{\#\#}P<0{\cdot}01$ vs HFD group.

Real-time PCR analysis showed that HFD-induced expression of TNF-α and MCP1 was significantly suppressed by BPS treatment (Fig. 3E and F). We could not detect serum TNF-α even in mice fed a HFD (data not shown).

BPS attenuated HFD-induced hepatic steatosis

Finally, we examined whether BPS affects hepatic steatosis induced by the HFD. HFD feeding for 12 weeks caused fatty liver compared with control feeding (Fig. 4A and B). Fat accumulation in the liver was attenuated in the BPS group compared with the HFD group (Fig. 4C and D).

Discussion

We demonstrated in this study that BPS improved HFD-induced insulin resistance and glucose intolerance. Treatment with BPS reduced expression of inflammatory cytokines, adipocyte size, and macrophage infiltration in WAT of diet-induced obesity mice. BPS also induced modest PPARγ upregulation. Although BPS treatment did not affect serum glucose and insulin levels after 16 h of fasting (Table 2), GTT performed after 6 h of fasting showed a significant reduction in basal glucose levels in the BPS group. The difference may be ascribed to the length of the fasting period, and prolonged fasting time may attenuate the difference between the HFD group and the BPS group.

Low-grade adipose tissue inflammation is a key state underlying insulin resistance in obesity. An increase in *TNF-α* mRNA expression was observed in adipose tissue from animal models of obesity and diabetes (Hotamisligil *et al.* 1993). It has been suggested that TNF-α is an important mediator of insulin resistance in obesity because neutralization of TNF-α increased peripheral glucose uptake in response to insulin in obese rats. And TNF-α-deficient obese mice were protected against obesity-induced attenuation of insulin signaling in muscle and fat tissues (Uysal *et al.* 1997). Several studies suggest that TNF-α blocks insulin signaling. It is reported that TNF-α inhibits insulin-induced tyrosine phosphorylation and tyrosine kinase activity of the insulin receptor in the obese rat (Hotamisligil *et al.* 1994*a*,*b*). TNF-α activates JNK signaling, and JNK activation promotes the

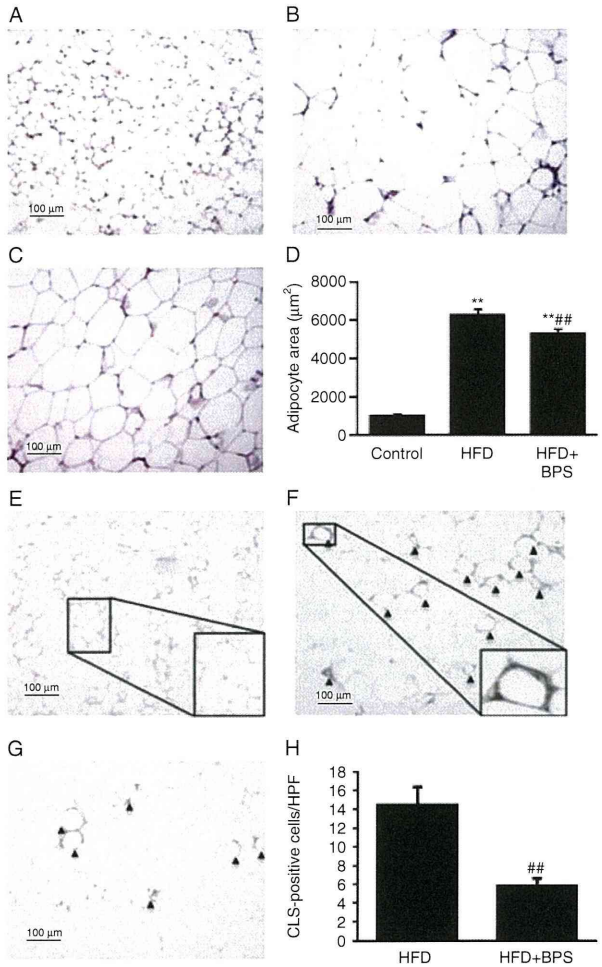

Figure 2 BPS treatment decreased adipocyte size and infiltration of macrophages in WAT. (A, B, and C) Representative microphotographs of H&E-stained sections of epididymal WAT from the control group (A), HFD group (B), and BPS group (C) are shown. Scale bar, 100 μm. (D) Bar graph indicates average adipocyte size of epididymal WAT, $n=5$ (control group; $n=3$). $^{**}P<0{\cdot}01$ vs control. $^{\#\#}P<0{\cdot}01$ vs HFD group. (E, F, and G) Representative microphotographs of WAT immunohistochemically stained with an anti-MAC3 antibody to stain macrophage in the control group (E), HFD group (F), and BPS group (G) are shown. Scale bar, 100 μm. (H) Bar graph indicates the number of CLSs in high power field (HPF), $n=7$–8. $^{\#\#}P<0{\cdot}01$ vs HFD group. Almost no CLS was observed in the control group.

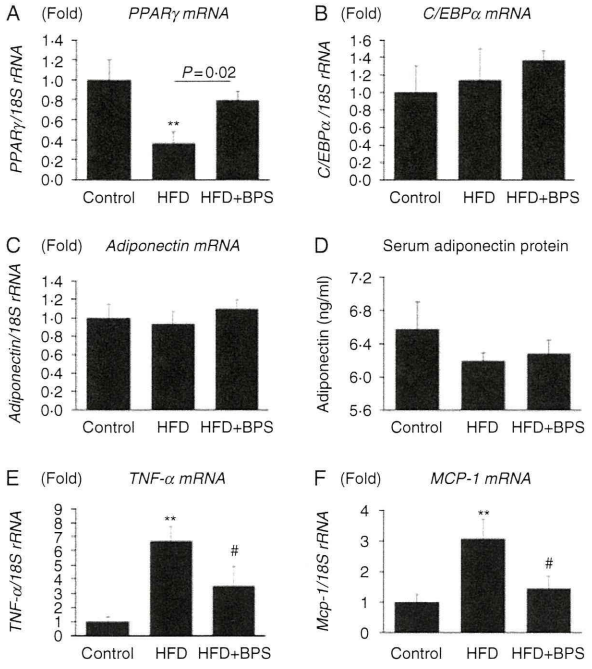

Figure 3 Effect of BPS on the adipocyte differentiation markers in WAT. (A, B and C) The results of real-time qPCR analysis for PPARγ (A), C/EBPα (B), and adiponectin (C) are shown, $n=5$. $^{**}P<0{\cdot}01$ vs control. (D) Serum adiponectin levels were determined by ELISA. (E and F) The results of real-time qPCR analysis for TNF-α (E) and MCP1 (F) expression in WAT are shown, $n=5$. $^{**}P<0{\cdot}01$ vs control. $^{\#}P<0{\cdot}05$ vs HFD group.

phosphorylation of IRS1 at serine residues that negatively regulate normal signaling through IRS1 (Aguirre *et al.* 2000, Shoelson *et al.* 2006). An absence of JNK1 (MAPK8) improved insulin sensitivity and enhanced insulin receptor signaling in diet-induced obesity mice and *ob/ob* genetic obesity mice (Hotamisligil *et al.* 1993, Hirosumi *et al.* 2002). In this study, BPS reduced mRNA expression of TNF-α in WAT from diet-induced obesity mice. Hence, we assume that reduction of TNF-α may contribute to the improvement of insulin action by BPS, at least in part. It is also expected that the signaling pathways activated by TNF-α are attenuated in the adipose tissue of BPS-treated mice. However, the effect of BPS seems to be multi-fold, such as reduction of MCP1. Therefore, it is difficult to determine specifically whether TNF-α-signaling is attenuated in this model. It is important to note that we must be cautious in extrapolating the data in this study to humans because TNF-α neutralizing antibodies have been shown to be ineffective on impacting insulin sensitivity in humans (Ofei *et al.* 1996).

Several studies showed anti-inflammatory effects of BPS. Ohta *et al.* (2005) showed that BPS suppressed concanavalin-A-induced TNF-α and INF-γ production and liver injury. It is also reported that BPS prevented the development of cigarette smoke extract-induced emphysema (Chen *et al.* 2009). Production of TNF-α and interleukin 1β (ILβ) in the lung tissue was suppressed by BPS in this model. Although activation of prostacyclin receptor is suggested to be involved in the anti-inflammatory effect, the detailed mechanism of BPS suppression of inflammatory cytokine production is not clear and further study is needed.

Hypertrophied adipose tissue secretes MCP1 (Hotamisligil *et al.* 1995, Bruun *et al.* 2005). MCP1 attracts macrophages to adipose tissue (Kamei *et al.* 2006). It is suggested that infiltrated macrophages secrete MCP1 and proinflammatory cytokines such as TNF-α or IL6, indicating that macrophage infiltration and inflammation of WAT form a vicious circle (Suganami *et al.* 2005). It is also reported that transgenic overexpression of MCP1 in adipose tissue causes insulin resistance by direct attenuation of insulin signaling in skeletal muscle and liver and inflammation of adipose tissue (Kamei *et al.* 2006, Kanda *et al.* 2006). Therefore, MCP1 is thought to contribute to insulin resistance through paracrine and endocrine effects (Kamei *et al.* 2006). BPS reduced both MCP1 expression and macrophage infiltration, which may contribute to the improvement of glucose tolerance and insulin action.

PPARγ has been known as a master regulator of adipocyte differentiation *in vivo* and *in vitro* (Rosen *et al.* 1999, Camp *et al.* 2002). PPARγ ligands, such as thiazolidinediones, improve insulin sensitivity by increasing the number of small adipocytes secreting adiponectin and decrease the number of large adipocytes secreting TNF-α in WAT (Okuno *et al.* 1998, Yamauchi *et al.* 2001). We observed that treatment with BPS decreased the average size of adipocytes in epididymal WAT from diet-induced obese mice. Although statistical significance was marginal, it is plausible to assume that the increased PPARγ by BPS may contribute to adipocyte

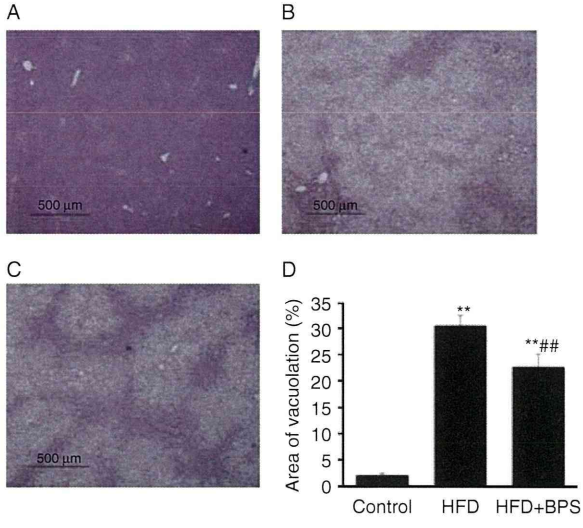

Figure 4 BPS attenuated HFD-induced hepatic steatosis. (A, B, and C) Representative microphotographs of H&E-stained sections of liver from the control group (A), HFD group (B), and BPS group (C) are shown. Scale bar, 500 μm. (D) Bar graph indicates area of vacuolation, $n=5$–8. $^{**}P<0{\cdot}01$ vs control. $^{\#\#}P<0{\cdot}01$ vs HFD group.

differentiation and improvement of insulin action. Because PPARγ is known to inhibit NF-κB, a transcription factor-mediating expression of inflammatory cytokines, BPS may suppress TNF-α and MCP1 expression through PPARγ activation. Although the detailed mechanism of BPS upregulation of PPARγ is not clear, a previous report showed that another prostacyclin analogue, treprostinil, activates PPARγ through prostacyclin receptor-dependent and cAMP-independent mechanisms (Falcetti *et al.* 2007).

Adipocytes become hypertrophied as obesity progresses. It is suggested that these hypertrophied adipocytes secrete free fatty acid that contributes to fat accumulation in ectopic sites including liver and muscle, leading to the development of insulin resistance (Jacob *et al.* 1999, Bays *et al.* 2004, Hwang *et al.* 2007). Although the mechanism is not clear, BPS mildly decreased serum TC and TG levels (Table 2). A decrease in the serum TC and TG levels by BPS may contribute to the improvement of insulin action.

It is of note that BPS ameliorated hepatic steatosis induced by HFD. Although the precise mechanism is not clear, anti-inflammatory effects of BPS may play a role in the attenuation of hepatic steatosis because recent studies suggest that inflammation is one of the critical factors in the development of hepatic steatosis. It was reported that anti-TNFα antibody treatment improved hepatic steatosis in *ob/ob* mice (Li *et al.* 2003). Treatment with an inhibitor of MCP1 receptor reportedly attenuated insulin resistance and hepatic steatosis in diet-induced obese mice (Tamura *et al.* 2010). Therefore, reduction of fat accumulation in the liver by BPS treatment may be due to suppression of inflammatory cytokine expression, at least in part, as observed in WAT of the BPS group. However, it is not clear at this point whether cytokine levels in the liver are decreased in the BPS group, and further study is needed.

A recent study showed that BPS improves glucose metabolism in a genetic obesity-induced insulin resistance model (Sato *et al.* 2010). Although our data mostly agree with those by Sato *et al.* (2010), our study is also important because we showed beneficial effects of BPS on glucose metabolism in a diet-induced obesity model, which is more clinically relevant than a genetic model. In addition, our data suggest a possible involvement of anti-inflammatory effects of BPS in the improvement of impaired glucose metabolism, which was not obvious in the previous study by Sato *et al.* (2010).

Taken together, we showed in this study that BPS improved glucose tolerance in mice fed a HFD possibly through suppression of inflammatory cytokines in WAT and induction of adipocyte differentiation. BPS may be beneficial not only for the treatment of patients with peripheral artery disease or pulmonary hypertension but also for treatment of patients with insulin resistance.

Declaration of interest

The authors declare that there is no conflict of interest that could be perceived as prejudicing the impartiality of the research reported.

Funding

This work was supported in part by a grant-in-aid for scientific research from the Ministry of Education, Culture, Sports, Science and Technology of Japan (19590867 to T I).

Author contribution statement

E I researched the data, contributed to discussion, wrote and reviewed/edited the manuscript. T I contributed to discussion and wrote and reviewed/edited the manuscript. K T and K S reviewed/edited the manuscript. H M, T H, J I, and A K researched the data.

Acknowledgement

The authors would like to thank the technical expertise of the Support Center for Education and Research, Kyushu University.

References

Aguirre V, Uchida T, Yenush L, Davis R & White MF 2000 The c-Jun NH(2)-terminal kinase promotes insulin resistance during association with insulin receptor substrate-1 and phosphorylation of Ser(307). *Journal of Biological Chemistry* **275** 9047–9054. (doi:10.1074/jbc.275.12.9047)

Bays H, Mandarino L & DeFronzo R 2004 Role of the adipocyte, free fatty acids, and ectopic fat in pathogenesis of type 2 diabetes mellitus: peroxisomal proliferator-activated receptor agonists provide a rational therapeutic approach. *Journal of Clinical Endocrinology and Metabolism* **89** 463–478. (doi:10.1210/jc.2003-030723)

Bruun JM, Lihn AS, Pedersen SB & Richelsen B 2005 Monocyte chemoattractant protein-1 release is higher in visceral than subcutaneous human adipose tissue (AT): implication of macrophages resident in the AT. *Journal of Clinical Endocrinology and Metabolism* **90** 2282–2289. (doi:10.1210/jc.2004-1696)

Camp HS, Ren D & Leff T 2002 Adipogenesis and fat-cell function in obesity and diabetes. *Trends in Molecular Medicine* **8** 442–447. (doi:10.1016/S1471-4914(02)02396-1)

Chen Y, Hanaoka M, Chen P, Droma Y, Voelkel NF & Kubo K 2009 Protective effect of beraprost sodium, a stable prostacyclin analog, in the development of cigarette smoke extract-induced emphysema. *American Journal of Physiology. Lung Cellular and Molecular Physiology* **296** L648–L656. (doi:10.1152/ajplung.90270.2008)

Falcetti E, Flavell DM, Staels B, Tinker A, Haworth SG & Clapp LH 2007 IP receptor-dependent activation of PPARgamma by stable prostacyclin analogues. *Biochemical and Biophysical Research Communications* **360** 821–827. (doi:10.1016/j.bbrc.2007.06.135)

Fujiwara K, Nagasaka A, Nagata M, Yamamoto K, Imamura S, Oda N, Sawai Y, Hayakawa N, Suzuki A & Itoh M 2004 A stable prostacyclin analogue reduces high serum TNF-alpha levels in diabetic patients. *Experimental and Clinical Endocrinology & Diabetes* **112** 390–394. (doi:10.1055/s-2004-821024)

Goya K, Otsuki M, Xu X & Kasayama S 2003 Effects of the prostaglandin I_2 analogue, beraprost sodium, on vascular cell adhesion molecule-1 expression in human vascular endothelial cells and circulating vascular cell adhesion molecule-1 level in patients with type 2 diabetes mellitus. *Metabolism* **52** 192–198. (doi:10.1053/meta.2003.50025)

Hirosumi J, Tuncman G, Chang L, Gorgun CZ, Uysal KT, Maeda K, Karin M & Hotamisligil GS 2002 A central role for JNK in obesity and insulin resistance. *Nature* **420** 333–336. (doi:10.1038/nature01137)

Hotamisligil GS, Shargill NS & Spiegelman BM 1993 Adipose expression of tumor necrosis factor-alpha: direct role in obesity-linked insulin resistance. *Science* **259** 87–91. (doi:10.1126/science.7678183)

Hotamisligil GS, Murray DL, Choy LN & Spiegelman BM 1994*a* Tumor necrosis factor alpha inhibits signaling from the insulin receptor. *PNAS* **91** 4854–4858. (doi:10.1073/pnas.91.11.4854)

Hotamisligil GS, Budavari A, Murray D & Spiegelman BM 1994*b* Reduced tyrosine kinase activity of the insulin receptor in obesity-diabetes. Central role of tumor necrosis factor-alpha. *Journal of Clinical Investigation* **94** 1543–1549. (doi:10.1172/JCI117495)

Hotamisligil GS, Arner P, Caro JF, Atkinson R & Spiegelman BM 1995 Increased adipose tissue expression of tumor necrosis factor-alpha in human obesity and insulin resistance. *Journal of Clinical Investigation* **95** 2409–2415. (doi:10.1172/JCI117936)

Hotamisligil GS, Peraldi P, Budavari A, Ellis R, White MF & Spiegelman BM 1996 IRS-1-mediated inhibition of insulin receptor tyrosine kinase activity in TNF-alpha- and obesity-induced insulin resistance. *Science* **271** 665–668. (doi:10.1126/science.271.5249.665)

Hwang JH, Stein DT, Barzilai N, Cui MH, Tonelli J, Kishore P & Hawkins M 2007 Increased intrahepatic triglyceride is associated with peripheral insulin resistance: *in vivo* MR imaging and spectroscopy studies. *American Journal of Physiology. Endocrinology and Metabolism* **293** E1663–E1669. (doi:10.1152/ajpendo.00590.2006)

Jacob S, Machann J, Rett K, Brechtel K, Volk A, Renn W, Maerker E, Matthaei S, Schick F, Claussen CD *et al.* 1999 Association of increased intramyocellular lipid content with insulin resistance in lean nondiabetic offspring of type 2 diabetic subjects. *Diabetes* **48** 1113–1119. (doi:10.2337/diabetes.48.5.1113)

Kamei N, Tobe K, Suzuki R, Ohsugi M, Watanabe T, Kubota N, Ohtsuka-Kowatari N, Kumagai K, Sakamoto K, Kobayashi M *et al.* 2006 Overexpression of monocyte chemoattractant protein-1 in adipose tissues causes macrophage recruitment and insulin resistance. *Journal of Biological Chemistry* **281** 26602–26614. (doi:10.1074/jbc.M601284200)

Kanda H, Tateya S, Tamori Y, Kotani K, Hiasa K, Kitazawa R, Kitazawa S, Miyachi H, Maeda S, Egashira K *et al.* 2006 MCP-1 contributes to macrophage infiltration into adipose tissue, insulin resistance, and hepatic steatosis in obesity. *Journal of Clinical Investigation* **116** 1494–1505. (doi:10.1172/JCI26498)

Li Z, Yang S, Lin H, Huang J, Watkins PA, Moser AB, Desimone C, Song XY & Diehl AM 2003 Probiotics and antibodies to TNF inhibit inflammatory activity and improve nonalcoholic fatty liver disease. *Hepatology* **37** 343–350. (doi:10.1053/jhep.2003.50048)

Masuzaki H, Paterson J, Shinyama H, Morton NM, Mullins JJ, Seckl JR & Flier JS 2001 A transgenic model of visceral obesity and the metabolic syndrome. *Science* **294** 2166–2170. (doi:10.1126/science.1066285)

Ofei F, Hurel S, Newkirk J, Sopwith M & Taylor R 1996 Effects of an engineered human anti-TNF-alpha antibody (CDP571) on insulin sensitivity and glycemic control in patients with NIDDM. *Diabetes* **45** 881–885. (doi:10.2337/diabetes.45.7.881)

Ohta S, Nakamuta M, Fukushima M, Kohjima M, Kotoh K, Enjoji M & Nawata H 2005 Beraprost sodium, a prostacyclin (PGI) analogue, ameliorates concanavalin A-induced liver injury in mice. *Liver International* **25** 1061–1068. (doi:10.1111/j.1478-3231.2005.01143.x)

Okuno A, Tamemoto H, Tobe K, Ueki K, Mori Y, Iwamoto K, Umesono K, Akanuma Y, Fujiwara T, Horikoshi H *et al.* 1998 Troglitazone increases the number of small adipocytes without the change of white adipose tissue mass in obese Zucker rats. *Journal of Clinical Investigation* **101** 1354–1361. (doi:10.1172/JCI1235)

Olschewski H, Rose F, Schermuly R, Ghofrani HA, Enke B, Olschewski A & Seeger W 2004 Prostacyclin and its analogues in the treatment of pulmonary hypertension. *Pharmacology & Therapeutics* **102** 139–153. (doi:10.1016/j.pharmthera.2004.01.003)

Rosen ED, Sarraf P, Troy AE, Bradwin G, Moore K, Milstone DS, Spiegelman BM & Mortensen RM 1999 PPAR gamma is required for the differentiation of adipose tissue *in vivo* and *in vitro*. *Molecular Cell* **4** 611–617. (doi:10.1016/S1097-2765(00)80211-7)

Sato N, Kaneko M, Tamura M & Kurumatani H 2010 The prostacyclin analog beraprost sodium ameliorates characteristics of metabolic syndrome in obese Zucker (fatty) rats. *Diabetes* **59** 1092–1100. (doi:10.2337/db09-1432)

Savage DB, Petersen KF & Shulman GI 2007 Disordered lipid metabolism and the pathogenesis of insulin resistance. *Physiological Reviews* **87** 507–520. (doi:10.1152/physrev.00024.2006)

Shoelson SE, Lee J & Goldfine AB 2006 Inflammation and insulin resistance. *Journal of Clinical Investigation* **116** 1793–1801. (doi:10.1172/JCI29069)

Suganami T, Nishida J & Ogawa Y 2005 A paracrine loop between adipocytes and macrophages aggravates inflammatory changes: role of free fatty acids and tumor necrosis factor alpha. *Arteriosclerosis, Thrombosis, and Vascular Biology* **25** 2062–2068. (doi:10.1161/01.ATV.0000183883.72263.13)

Tamura Y, Sugimoto M, Murayama T, Minami M, Nishikaze Y, Ariyasu H, Akamizu T, Kita T, Yokode M & Arai H 2010 C–C chemokine receptor 2 inhibitor improves diet-induced development of insulin resistance and hepatic steatosis in mice. *Journal of Atherosclerosis and Thrombosis* **17** 219–228. (doi:10.5551/jat.3368)

Uysal KT, Wiesbrock SM, Marino MW & Hotamisligil GS 1997 Protection from obesity-induced insulin resistance in mice lacking TNF-alpha function. *Nature* **389** 610–614. (doi:10.1038/39335)

Wajchenberg BL 2000 Subcutaneous and visceral adipose tissue: their relation to the metabolic syndrome. *Endocrine Reviews* **21** 697–738. (doi:10.1210/er.21.6.697)

Watanabe M, Nakashima H, Mochizuki S, Abe Y, Ishimura A, Ito K, Fukushima T, Miyake K, Ogahara S & Saito T 2009 Amelioration of diabetic nephropathy in OLETF rats by prostaglandin I(2) analog, beraprost sodium. *American Journal of Nephrology* **30** 1–11. (doi:10.1159/000195722)

Weisberg SP, McCann D, Desai M, Rosenbaum M, Leibel RL & Ferrante AW Jr 2003 Obesity is associated with macrophage accumulation in adipose tissue. *Journal of Clinical Investigation* **112** 1796–1808. (doi:10.1172/JCI19246)

Weisberg SP, Hunter D, Huber R, Lemieux J, Slaymaker S, Vaddi K, Charo I, Leibel RL & Ferrante AW Jr 2006 CCR2 modulates inflammatory and metabolic effects of high-fat feeding. *Journal of Clinical Investigation* **116** 115–124. (doi:10.1172/JCI24335)

Xu H, Barnes GT, Yang Q, Tan G, Yang D, Chou CJ, Sole J, Nichols A, Ross JS, Tartaglia LA *et al.* 2003 Chronic inflammation in fat plays a crucial role in the development of obesity-related insulin resistance. *Journal of Clinical Investigation* **112** 1821–1830. (doi:10.1172/JCI19451)

Yamauchi T, Kamon J, Waki H, Terauchi Y, Kubota N, Hara K, Mori Y, Ide T, Murakami K, Tsuboyama-Kasaoka N *et al.* 2001 The fat-derived hormone adiponectin reverses insulin resistance associated with both lipoatrophy and obesity. *Nature Medicine* **7** 941–946. (doi:10.1038/90984)

Received in final form 25 March 2012
Accepted 29 March 2012
Made available online as an Accepted Preprint
29 March 2012

Clinical SCIENCE

www.clinsci.org

online data

Clinical Science (2012) 123, 241–249 (Printed in Great Britain) doi:10.1042/CS20110633

Acetylcholinesterase inhibitors attenuate angiogenesis

Ryohei MIYAZAKI*, Toshihiro ICHIKI*†, Toru HASHIMOTO*, Jiro IKEDA*, Aya KAMIHARAGUCHI*, Eriko NARABAYASHI*, Hirohide MATSUURA*, Kotaro TAKEDA*† and Kenji SUNAGAWA*

*Departments of Cardiovascular Medicine, Kyushu University Graduate School of Medical Sciences, Fukuoka, Japan, and †Advanced Therapeutics for Cardiovascular Diseases, Kyushu University Graduate School of Medical Sciences, Fukuoka, Japan

ABSTRACT

Donepezil {(*RS*)-2-[(1-benzyl-4-piperidyl)methyl]-5,6-dimethoxy-2,3-dihydroinden-1-one} is a reversible acetylcholinesterase inhibitor and used for treatment of patients with AD (Alzheimer's disease). Recent studies showed that treatment with donepezil reduced production of inflammatory cytokines in PBMCs (peripheral blood mononuclear cells). It was also reported that muscle-derived inflammatory cytokines play a critical role in neovascularization in a hindlimb ischaemia model. We sought to determine whether donepezil affects angiogenesis. A hindlimb ischaemia model was created by unilateral femoral artery ligation. Blood flow recovery examined by laser Doppler perfusion imaging and capillary density by immunohistochemical staining of CD31-positive cells in the ischaemic hindlimb were significantly decreased in donepezil- and physostigmine-treated mice compared with control mice after 2 weeks. Donepezil reduced expression of IL (interleukin)-1β and VEGF (vascular endothelial growth factor) in the ischaemic hindlimb. Intramuscular injections of IL-1β to the ischaemic hindlimb reversed the donepezil-induced VEGF down-regulation and the anti-angiogenic effect. Hypoxia induced IL-1β expression in C2C12 myoblast cells, which was inhibited by pre-incubation with ACh (acetylcholine) or LY294002, a PI3K (phosphoinositide 3-kinase) inhibitor. Donepezil inhibited phosphorylation of Akt [also known as PKB (protein kinase B)], a downstream kinase of PI3K, in the ischaemic hindlimb. These findings suggest that cholinergic stimulation by acetylcholinesterase inhibitors suppresses angiogenesis through inhibition of PI3K-mediated IL-1β induction, which is followed by reduction of VEGF expression. Acetylcholinesterase inhibitor may be a novel anti-angiogenic therapy.

INTRODUCTION

Donepezil {(*RS*)-2-[(1-benzyl-4-piperidyl)methyl]-5,6-dimethoxy-2,3-dihydroinden-1-one} is a specific and reversible acetylcholinesterase inhibitor that increases bioavailability of ACh (acetylcholine), a neurotransmitter both in the CNS (central nervous system) and PNS (peripheral nervous system). Donepezil is used for

Key words: acetylcholinesterase inhibitor, angiogenesis, hindlimb ischaemia, interleukin-1β.

Abbreviations: ACh, acetylcholine; AD, Alzheimer's disease; bFGF, basic fibroblast growth factor; BP, blood pressure; CNS, central nervous system; COPD, chronic obstructive pulmonary disease; DMEM, Dulbecco's modified Eagle's medium; donepezil, (*RS*)-2-[(1-benzyl-4-piperidyl)methyl]-5,6-dimethoxy-2,3-dihydroinden-1-one; ERK, extracellular-signal-regulated kinase; FBS, fetal bovine serum; HPF, high-power field; HR, heart rate; IL, interleukin; JNK, c-Jun N-terminal kinase; LPS, lipopolysaccharide; mAChR, muscarinic ACh receptor; MAPK, mitogen-activated protein kinase; nAChR, nicotinic ACh receptor; NF-κB, nuclear factor κB; PBMC, peripheral blood mononuclear cell; PDGF, platelet-derived growth factor; PI3K, phosphoinositide 3-kinase; PTEN, phosphatase and tensin homologue deleted on chromosome 10; qRT–PCR, quantitative reverse transcription–PCR; TNFα, tumour necrosis factor α; VEGF, vascular endothelial growth factor.

Correspondence: Professor Toshihiro Ichiki (email ichiki@cardiol.med.kyushu-u.ac.jp).

treatment of patients with AD and known to improve cognitive function [1]. Treatment of the patients with AD with donepezil is associated with reduction in the serum cytokine level and cytokine production from PBMCs (peripheral blood mononuclear cells) [2], suggesting a possible anti-inflammatory effect of donepezil.

Recent studies suggest that ACh, a neurotransmitter of the vagus nerve, has an anti-inflammatory effect [3]. VNS (vagus nerve stimulation) attenuated TNFα (tumour necrosis factor α) secretion from macrophages and hypotension induced by LPS (lipopolysaccharide) [4]. ACh inhibits activation of NF-κB (nuclear factor κB) [5] and induces suppressor of cytokine signal 3 expression in macrophages [6], resulting in the attenuation of inflammatory responses. Therefore it is possible that acetylcholinesterase inhibitor attenuates inflammation through activation of this so-called cholinergic anti-inflammatory pathway.

Inflammation is a regulated response to harmful stimuli such as infection and ischaemic/hypoxic injury [7] and also plays a pivotal role in neovascularization [8]. The enhancement of angiogenesis by inflammation is partly explained by production of various angiogenic growth factors such as VEGF (vascular endothelial growth factor), bFGF (basic fibroblast growth factor), PDGF (platelet-derived growth factor) and MCP (monocyte chemoattractant protein)-1 from the leucocytes infiltrated into the ischaemic tissue [9]. It was also reported that IL (interleukin)-1β secreted from regenerating muscle after hindlimb ischaemia is critical for the enhanced neovascularization by implantation of PBMCs [10].

These studies prompted us to study the effect of cholinergic stimulation by donepezil on angiogenesis in a mouse model of hindlimb ischaemia. In the present study, we showed that pharmacological stimulation of cholinergic system by acetylcholinesterase inhibitors suppressed angiogenesis through inhibition of IL-1β induction.

MATERIALS AND METHODS

Materials

DMEM (Dulbecco's modified Eagle's medium) was purchased from Gibco BRL. FBS (fetal bovine serum) was from JRH Biosciences. Donepezil was purchased from Tronto Research Chemicals. ACh, physostigmine, heat-inactivated horse serum and BSA were purchased from Sigma. Mouse recombinant IL-1β was purchased from PeproTec. An anti-CD31 (PECAM1) antibody was purchased from Santa Cruz Biotechnology. Antibodies against ERK (extracellular-signal-regulated kinase), p38 MAPK (mitogen-activated protein kinase), JNK (c-Jun N-terminal kinase) and Akt and their phosphorylated (p) forms were obtained from Cell Signaling Technology. HRP (horseradish peroxidase)-conjugated secondary antibodies (anti-rabbit or anti-mouse IgG) were purchased from Vector Laboratories. SB203580 was a gift from GalxoSmithKline. PD98059 was purchased from BIOMOL Research Laboratories. LY294002 and SP600125 were purchased from Sigma. Other chemical reagents were purchased from Wako Pure Chemicals unless mentioned specifically.

Cell culture

C2C12 (mouse myoblast cell) cells were obtained from the RIKEN BioResource Center. C2C12 cells were maintained in low-glucose DMEM supplemented with 10% FBS (growth medium) at 37°C in a humidified atmosphere of 95% air/5% CO_2. C2C12 cells were grown to confluence, cultured in DMEM with 5% horse serum (differentiation medium) for additional 2 days and used in the experiment.

qRT–PCR (quantitative reverse transcription–PCR)

Total RNA was prepared by an acid guanidinium/phenol/chloroform extraction method with ISOGEN (Nippon Gene) according to the manufacturer's instructions. Then the total RNA (0.4 μg) was reverse-transcribed using moloney murine leukaemia virus RT (ReverTra Ace-α kit; Toyobo). The expression of mRNA was determined using SYBR-green (Toyobo) RT–PCR method and normalized to mouse β-actin expression. Primer sequences used in the present study are shown in Supplementary Table S1 (at http://www.clinsci.org/cs/123/cs1230241add.htm). ABI Prism 7500 Sequence Detection System (Applied Biosystems) was used.

Animal experiment

All procedures were approved by the institutional animal use and care committee and were conducted in conformity with institutional guidelines and Guide for Care and Use of Laboratory Animals (NIH Publication No. 85–23, revised 1996). Nine-week-old C57BL/6 mice were purchased from Kyudo. Mice were anaesthetized by a bolus intraperitoneal injection of ketamine (90 mg/kg of body weight) and xylazine (4 mg/kg of body weight), which allowed approximately 60 min of anaesthesia for creation of hindlimb ischaemia and implantation of osmotic minipumps. The adequacy of anaesthesia was monitored by confirming the absence of the movement of the mice during the surgical procedure. To produce hindlimb ischaemia, the proximal portion of the left femoral artery including the deep branches was ligated, followed by ligation of distal portion of saphenous artery. The artery and all side branches between two ligation sites were excised completely. Then the mice were allotted to the donepezil group, the physostigmine group or the control group in a random manner. Donepezil was

suspended in water, and administered *ad libitum*. The estimated dose of orally ingested donepezil was 10 mg/kg of body weight per day. Some of the donepezil-treated mice were given an intramuscular injection of 0.5 ng of mouse recombinant IL-1β to the ischaemic limb on days 3, 5 and 7 after the operation.

Physostigmine (2 mg/kg of body weight per day) was administered via an osmotic minipump (Alzet). Physostigmine [11] and donepezil [12] at doses used in this study were reported to inhibit brain acetylcholinesterase activity by 62 and 45 % respectively. Nicotine (approximately 12 mg/kg of body weight per day) and bethanechol (approximately 20 mg/kg of body weight per day) were orally administered. The doses of nicotine and bethanechol were determined based on previous studies [13,14]. BP (blood pressure) and HR (heart rate) were measured using tail-cuff method (UR-5000; Ueda). Hindlimb blood perfusion was measured by a laser Doppler perfusion imaging system (Moor Instruments LDI). Before imaging, mice were placed on a heating plate at 37 °C to minimize the influence of temperature. After 2 weeks, mice were killed with an overdose of pentobarbital anaesthesia and the gastrocnemial muscle was quickly removed.

Immunohistochemistry

The gastrocnemial muscle was harvested and fixed overnight in 10 % buffered-formaldehyde. After fixation, the tissue was embedded in paraffin and serial cross-sections of the muscle were used for immunohistochemical analysis. Paraffin sections were deparaffinized and then subjected to heat-induced antigen retrieval for 15 min at 90 °C in citrate buffer (pH 6.0). Blocking of the section was performed with 2 % BSA for 1 h at room temperature (25 °C). The sections were incubated with a rat monoclonal anti-CD31 (PECAM1) antibody diluted 1:200 in blocking solution at 4 °C, which was followed by incubation with Alexa Fluor® 555-conjugated rabbit anti-(rat IgG) diluted 1:1000 in blocking solution. After incubation, the sections were rinsed in PBS three times. The slides were immersed in 70 % ethanol supplemented with 0.1 % Sudan Black B for 15 min and washed 70 % ethanol twice to eliminate or reduce autofluorescence as described previously [15]. The specimens were observed under a confocal microscope. An independent investigator blind to the treatment of the samples counted the number of positive cells.

Western blotting

Western blot analysis was performed by a conventional method as described previously [16]. Phosphorylated Akt was detected using a phospho-Akt antibody. The protein expression was detected by ECL® (enhanced chemiluminescence; GE Healthcare) according to the manufacturer's instructions. Membranes were scanned using LAS-4000mini (Fujifilm). The membranes were stripped and reprobed with an antibody against Akt (which recognizes both phosphorylated and non-phosphorylated forms of Akt) by the same procedure. The level of phosphorylated Akt was normalized to that of total Akt. Activation of ERK, JNK and p38 MAPK was examined by the same method. Physostigmine, an acetylcholinesterase inhibitor (10 nmol/l), was added to circumvent the effect of acetylcholinesterase in the culture medium for *in vitro* study.

ELISA

The serum of the mouse was collected and frozen at − 80 °C until assay. Concentrations of IL-1β, IL-6, TNFα and VEGF were determined by ELISA using appropriate commercial kits (R&D Systems). The gastrocnemial muscle of the ischaemic limb lysed in sample buffer of Western blot analysis was also subjected to ELISA for cytokine measurement.

Statistical analysis

Statistical analysis was performed with one-way ANOVA and Fisher test, if appropriate. Results are shown as means ± S.E.M. $P < 0.05$ was considered to be statistically significant.

RESULTS

Inhibition of angiogenesis by acetylcholinesterase inhibitors

Laser Doppler perfusion imaging revealed a rapid decrease and gradual recovery of the ischaemic/non-ischaemic hindlimb perfusion ratio after ligation of unilateral femoral artery (Figures 1A and 1B). The blood flow recovery of the hindlimb was significantly attenuated in donepezil-treated mice. Physostigmine, another acetylcholinesterase inhibitor that is structurally different from donepezil, also attenuated blood flow recovery, indicating that activation of cholinergic system attenuates angiogenesis in the hindlimb. Consistent with the results of laser Doppler perfusion analysis, treatment with donepezil or physostigmine significantly decreased the capillary density immunohistochemically evaluated with an anti-CD31 antibody in the ischaemic hindlimb (Figures 1C and 1D).

BP and body weight were not significantly different between acetylcholinesterase inhibitor-treated mice and control mice after 2 weeks of unilateral femoral artery ligation (see Supplementary Table S2 at http://www.clinsci.org/cs/123/cs1230241add.htm). Treatment with donepezil significantly reduced HR. However, physostigmine at the dose we used did not affect HR, indicating that HR reduction does not play a major role in the attenuation of blood flow recovery.

We then determined the effect of the specific agonist of mAChR (muscarinic ACh receptor; bethanechol) or

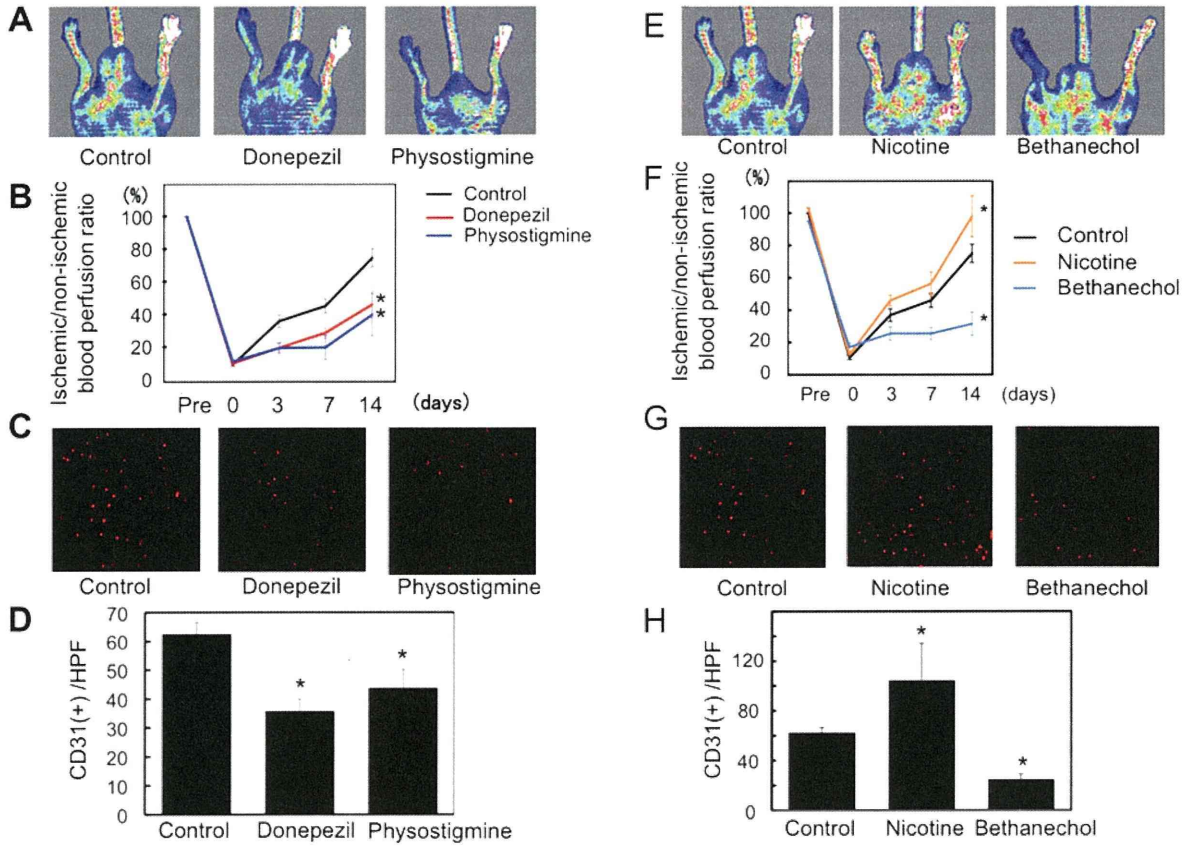

Figure 1 Acetylcholinesterase inhibitors attenuate neovascularization in a mouse model of hindlimb ischaemia

The effect of donepezil or physostigmine on blood flow recovery after hindlimb ischaemia was examined (A–D). The effect of bethanechol or nicotine on blood flow recovery after hindlimb ischaemia was examined (E–H). (A, E), Representative laser Doppler perfusion images of blood flow after 2 weeks of hindlimb ischaemia are shown. (B, F) Ratio of blood flow in the ischaemic hindlimb to that in the non-ischaemic hindlimb measured immediately (day 0) and at the days indicated in the Figure after unilateral femoral artery ligation. (C, G) Immunohistochemical staining for CD31 in the gastrocnemial muscle of ischaemic hindlimb is shown. (D, H) Capillary density expressed as the number of capillaries per HPF (high-power field). Results are expressed as means ± S.E.M. ($n = 7$). $^*P < 0.05$ compared with the control group.

nAChR (nicotinic ACh receptor; nicotine) on the blood flow recovery and capillary density of the ischaemic hindlimb (Figures 1E–1H). Bethanechol reduced blood flow recovery and capillary density of the ischaemic hindlimb, suggesting that mAChR is responsible for the attenuation of blood flow recovery by cholinergic stimulation. In contrast, nicotine enhanced blood flow recovery. Although the mechanism is not clear, the net effect of acetylcholinesterase inhibitors on angiogenesis favours mAChR stimulation in our model.

Donepezil suppressed VEGF and IL-1β expression in the ischaemic hindlimb

mRNA expression of angiogenic factors and cytokines in the ischaemic hindlimb harvested at day 7 was examined (Figure 2A). The expression of VEGF mRNA was significantly decreased in the donepezil-treated mice. However, expression of other angiogenic factors including bFGF, PDGF, PLGF (placental growth factor), Angpt (angiopoietin) 1 and 2 was not affected by donepezil treatment. Expression of IL-1β and TNFα mRNA in the ischaemic hindlimb was significantly decreased in the donepezil-treated group, suggesting an anti-inflammatory effect of donepezil. qRT–PCR also showed a trend towards reduction of CD3ε (T-lymphocytes) and F4/80 (macrophages) mRNA in the ischaemic hindlimb of the donepezil-treated mice compared with that of control mice. Although the difference was not statistically significant, the results suggest that treatment with donepezil mildly suppressed infiltration of inflammatory cells into the ischaemic hindlimb.

Protein level of IL-1β was significantly suppressed in an ischaemic hindlimb of donepezil-treated mice (Figure 2B). Although VEGF level was also decreased in an ischaemic hindlimb of donepezil-treated mice, the difference of VEGF level between control and donepezil-treated mice showed a borderline significance. We could not detect any changes in the serum levels of IL-1β, IL-6,

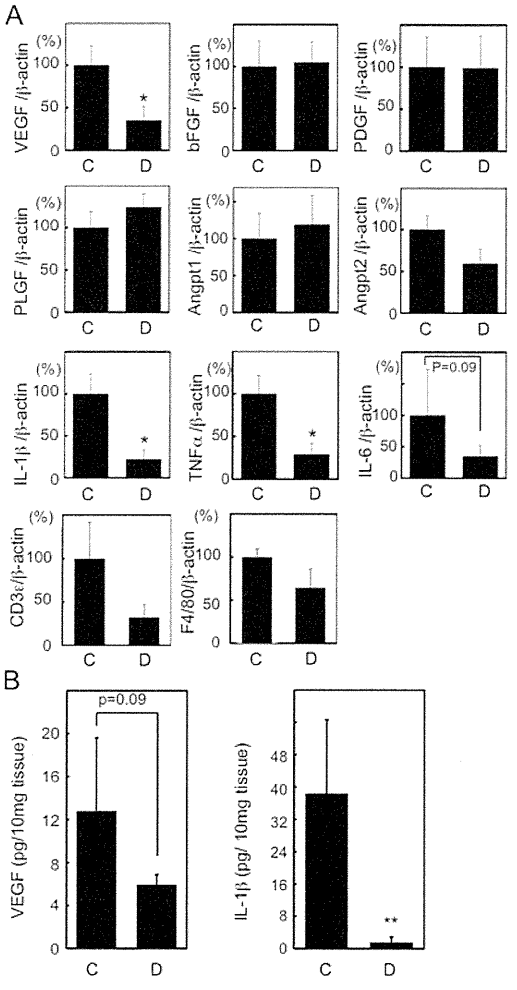

Figure 2 mRNA and protein expression in the ischaemic hindlimb of control and donepezil-treated mice

(A) mRNA expression of angiogenic factors and inflammatory cytokines in the ischaemic hindlimb of control (bar C) and donepezil-treated (bar D) mice was quantified with real time RT–PCR. The primer sequences used are indicated in Supplementary Table S1 at http://www.clinsci.org/cs/123/cs1230241add.htm. The expression level of each mRNA in the ischaemic hindlimb of control mouse was set as 100 % ($n = 7$). $^*P < 0.05$ compared with the control group. (B) Protein level of IL-1β and VEGF in the ischaemic hindlimb of control and donepezil-treated mice was measured by ELISA ($n = 4$). $^*P < 0.05$ compared with the control group.

or VEGF (results not shown). TNFα was not detectable in the serum and in ischaemic hindlimb in both groups. These findings suggest that donepezil locally suppressed inflammation in an ischaemic hindlimb.

IL-1β reversed the anti-angiogenic effect of donepezil

A previous report showed that recipient-derived IL-1β plays an important role in blood flow recovery in the ischaemic hindlimb [10,17]. As IL-1β expression was decreased in the ischaemic hindlimb of the donepezil-treated mice, we injected recombinant murine IL-1β into the ischaemic hindlimb. An injection of IL-1β restored the reduced blood flow recovery (Figures 3A and 3B) and capillary formation (Figures 3C and 3D) in the donepezil-treated mice. Donepezil-induced suppression of VEGF mRNA expression in the ischaemic hindlimb was also reversed by the IL-1β injection (Figure 3E). The IL-1β injection did not cause haemodynamic changes (see Supplementary Table S3 at http://www.clinsci.org/cs/123/cs1230241add.htm).

Role of PI3K (phosphoinositide 3-kinase) pathway in hypoxia-induced IL-1β induction

To gain an insight into the mechanism of donepezil inhibition of IL-1β expression, we used C2C12 cells, a mouse embryonic myoblast cell line. As hindlimb muscles are exposed to hypoxic conditions after femoral artery ligation, the effect of low oxygen concentration (1 % O_2) on IL-1β mRNA expression was determined. After exposure to the hypoxic condition for 12 h, IL-1β mRNA level was significantly increased compared with that in C2C12 cells incubated in normoxic (20 % O_2) conditions (Figure 4A). The induction of IL-1β by hypoxic conditions was significantly inhibited by pre-incubation with ACh. The Ach-induced suppression of IL-1β was reversed by the presence of atropine, a competitive antagonist of mAChR, but not by mecamylamine, a specific antagonist of nAChR. These results indicate that mAChR is responsible for the suppression of hypoxia-induced IL-1β expression. The findings are consistent with the *in vivo* results that a mAChR agonist bethanechol inhibited angiogenesis.

It was reported that PI3K and MAPKs are involved in IL-1β induction [18]. Treatment with LY294002 (PI3K inhibitor), PD98059 (ERK kinase inhibitor) or SP600125 (JNK inhibitor) significantly decreased hypoxia-induced IL-1β mRNA expression (Figure 4B). ACh attenuated hypoxia-induced phosphorylation of Akt, a downstream kinase of PI3K, but did not affect phosphorylation of ERK, JNK or p38 MAPK in C2C12 cells (Figures 4C–4F). These results suggest that ACh may suppress hypoxia-induced IL-1β expression through inhibition of the PI3K/Akt pathway. Indeed, the phosphorylation level of Akt but not other MAPKs was decreased in the ischaemic hindlimb of donepezil-treated mice (Figures 4G–4J).

DISCUSSION

We have shown in the present study that treatment with donepezil attenuated blood flow recovery of the ischaemic hindlimb in mice through reduction of the expression of IL-1β. It was suggested that mAChR is involved in this process. ACh as well as PI3K inhibitor suppressed hypoxia-induced IL-1β induction

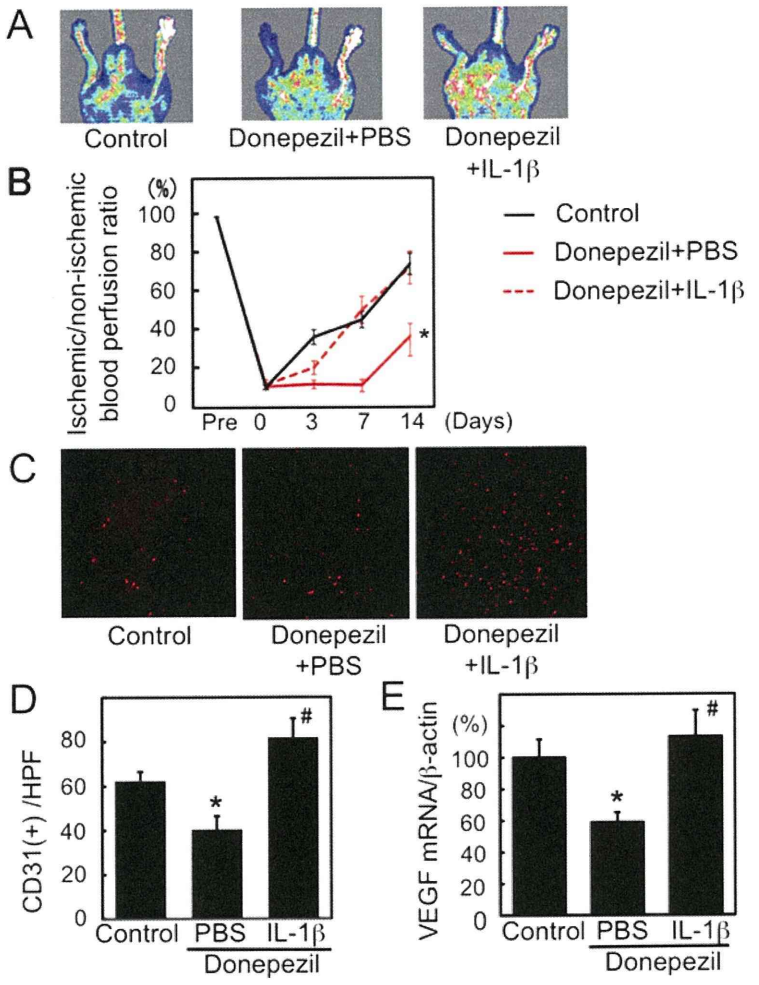

Figure 3 **IL-1β reverses donepezil-induced inhibition of neovascularization**

(A) Representative laser Doppler perfusion images of blood flow in the ischaemic hindlimb of donepezil-treated mice with or without IL-1β injection are shown. Control indicates ischaemic hindlimb without donepezil treatment. (B) Ratio of blood flow in the ischaemic hindlimb to that in the non-ischaemic hindlimb. $^{*}P < 0.05$ compared with control. (C) Immunohistochemical staining for CD31 in the gastrocnemial muscle of ischaemic hindlimb is shown. (D) Capillary density that is expressed as the number of capillaries per HPF. (E) mRNA expression of VEGF was quantified with real-time RT–PCR. Results are expressed as means $\pm$ S.E.M. ($n = 6-8$). $^{*}P < 0.05$ compared with control; $^{\#}P < 0.05$ compared with donepezil + PBS.

in C2C12 cells. Donepezil suppressed Akt activation in the ischaemic hindlimb, suggesting that an increase in Ach level by donepezil may inhibit hypoxia-induced IL-1β induction through suppression of the PI3K/Akt pathway, resulting in the inhibition of VEGF induction and angiogenesis.

A recent meta-analysis by Singh et al. [19] revealed that inhalation of anti-cholinergics is associated with a significant increase in the risk of cardiovascular events in patients with COPD (chronic obstructive pulmonary disease). Inhalation of anti-cholinergics significantly increased the risk of myocardial infarction and cardiovascular death without a statistically significant effect on the risk of stroke. This meta-analysis may support the idea that anti-cholinergics, contrary to acetylcholinesterase inhibitors, accelerate angiogenesis in the atherosclerotic plaque and thereby increase its vulnerability, which results in an increase in the cardiovascular events. However, a very recent double-blind trial that examined the effect of tiotropium, one of the anti-cholinergics, in patients with COPD showed opposite results [20]. Treatment with tiotropium showed an insignificant decrease in the number of death in patients with COPD and significantly decreased the incidence of myocardial infarction compared with placebo. Therefore the issue regarding the effect of anti-cholinergics treatment on cardiovascular events is still controversial.

Stimulation of nAChR is reported to enhance proliferation of endothelial cells and angiogenesis [13], which is consistent with the present study. Although stimulation of mAChR by bethanechol suppressed angiogenesis, the mechanism by which acetylcholinesterase inhibitors that

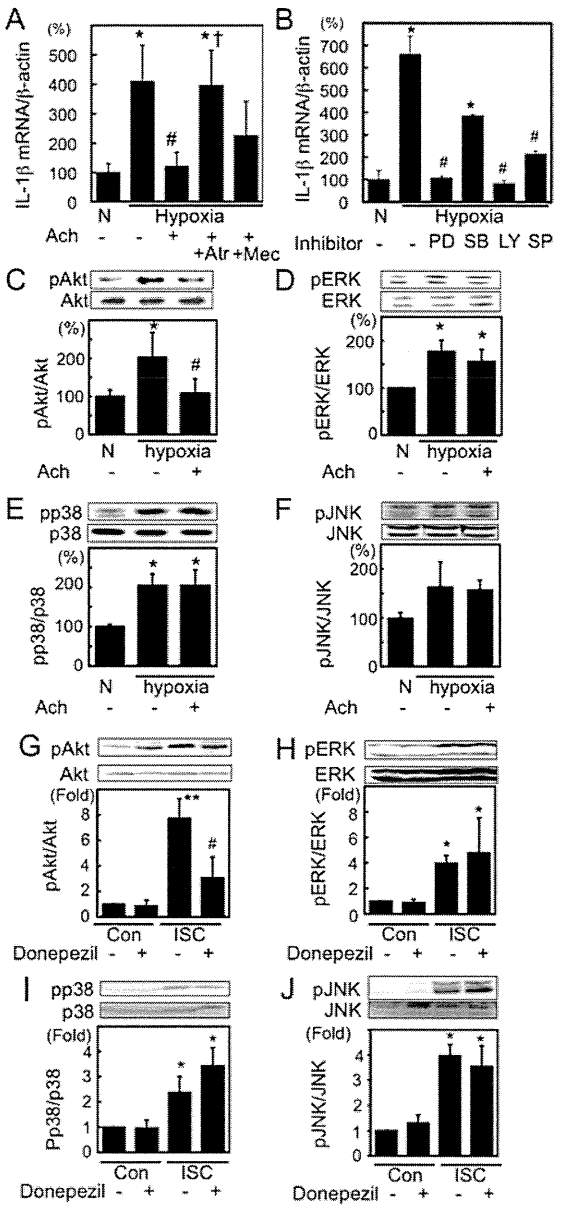

Figure 4 Ach and donepezil suppresses Akt activation

(A) C2C12 myoblast cells were pre-incubated with ACh (100 nmol/l) in the presence of atropine (Atr, 10 μmol/l) or mecamylamine (Mec, 10 μmol/l) prior to exposure to hypoxia (1 % O_2) for 1 h. After exposure to hypoxic condition for 12 h, the IL-1β mRNA level was determined with real time RT–PCR. N, normoxia. (B) The effects of PD98059 (PD; an ERK inhibitor, 10 μmol/l), SB203580 (SB; a p38 MAPK inhibitor, 10 μmol/l), LY294002 (LY; a PI3K inhibitor, 10 μmol/l) and SP600125 (SP; a JNK inhibitor, 10 μmol/l) on hypoxia-induced IL-1β mRNA expression in C2C12 cells were examined. mRNA expression of IL-1β in C2C12 cells cultured under normoxia (N) is used as control. $^{*}P < 0.05$ compared with under normoxic conditions; $^{\#}P < 0.05$ compared with hypoxia; $^{\dagger}P < 0.05$ compared with hypoxia + Ach ($n = 4$). (C–F) Effect of ACh on hypoxia-induced activation of Akt and MAPK was examined. (G–J) Effect of donepezil on the activation of Akt and MAPK in the non-ischaemic (Con) and ischaemic (ISC) hindlimb was examined. The ratio of phosphorylated form to total protein level of each kinase is shown in the histograms ($n = 4$). $^{*}P < 0.05$ compared with control, $^{\#}P < 0.05$ compared with the ischaemic hindlimb without donepezil.

are supposed to stimulate both nAChR and mAChR mimic the effect of mAChR is not clear.

Our *in vitro* results suggest that the increased ACh may be targeting ischaemic muscle of hindlimb, because Ach inhibited hypoxia-induced IL-1β expression in myoblast cells and donepezil reduced IL-1β expression in the ischaemic hindlimb. Therefore the anti-inflammatory effect of ACh on regenerating skeletal muscle may be dominant compared with direct effects of Ach on endothelial cells. Although we cannot exclude possible non-specific effects of these acetylcholinesterase inhibitors on angiogenesis, this is unlikely because the structure of donepezil and physostigmine is quite different.

The source of ACh in this hindlimb ischaemia model is not clear at this point. It is possible that an increase in ACh in the motor nerve ending of neuromuscular junction may play a role. Recent studies suggest that macrophages express choline acetyltransferase, which produces Ach from choline and acetyl-CoA [21]. Therefore infiltrated inflammatory cells may be another possible source of ACh. Alternatively, the ischaemic muscle itself may be the source of ACh, because it was previously reported that immunoreactivity of choline acetyltransferase is observed in both myoblasts and myotubes [22]. Another possibility is that acetylcholinesterase inhibitors may suppress angiogenesis in an indirect manner. mAChR in the CNS is reported to be involved in cholinergic anti-inflammatory pathway. Intracerebroventricular administration of muscarine, an agonist for mAChR, inhibited LPS-induced production of TNFα in the serum [23]. We cannot exclude the possible effect of these acetylcholinesterase inhibitors on the CNS in mediating an anti-angiogenic effect. Further study is needed to clarify the source and target cells of ACh in the ischaemic hindlimb.

A recent report showed that chronic hypoxia increased Akt phosphorylation in human macrophages [24]. Another report showed that TNFα-induced IL-1β expression is dependent on PI3K/Akt and NF-κB activation [18]. We showed that Ach suppressed hypoxia-induced IL-1β expression and Akt phosphorylation in C2C12 cells. And PI3K inhibitor suppressed hypoxia-induced IL-1β expression. Therefore it is suggested that Ach suppresses hypoxia-induced IL-1β expression through inhibition of PI3K/Akt pathway. Although it is known that PTEN (phosphatase and tensin homologue deleted on chromosome 10) negatively regulates PI3K/Akt pathway, we could not detect any change in PTEN expression in the ischaemic hindlimb in donepezil-treated mice (results not shown). The mechanism by which Ach inhibition of hypoxia-induced PI3K/Akt pathway is not clear and further study is needed.

The limitation of the present study is that the dose of donepezil used in this study is very high compared with

that clinically used for treatment of patients with AD. Therefore we must be cautious whether donepezil at a clinical dose affects angiogenesis in patients. A dose of 5–10 mg/kg of body weight per day of donepezil used in this study is widely used to examine the effect of donepezil on dementia in a rodent model [12] despite the fact that the clinical dose is 5–10 mg/day for patients with AD. It may be possible that differential susceptibility to the drug between humans and mice account for the requirement for high dose of donepezil in rodent models. A recent study showed a very small increase in skin temperature in the ischaemic hindlimb by donepezil, suggesting an angiogenic effect of donepezil [25]. The reason for the discrepancy between the previous study and our study is not clear at this point. However, the dose of donepezil administered to mice is higher in this study compared with the previous study (5 mg/kg of body weight per day), which may explain the discrepancy. Alternatively, the discrepancy may be because the previous report measured skin temperature rather than blood flow. In addition, the authors failed to examine the time course and measured surface temperature at later stage (28 days after ligation of femoral artery). We could not exclude the possibility that the difference of blood flow recovery of ischaemic hindlimb between control and donepezil-treated mice disappears or reverses after day 14 of femoral artery ligation. However, most of the study using C57BL/6 mice showed that blood flow recovery after hindlimb ischaemia reaches a plateau at day 14 or 21 [26,27]. Therefore this possibility is unlikely. And an anti-angiogenic effect of acetylcholinesterase inhibitor is confirmed by physostigmine in our study. Therefore it is suggested that acetylcholinesterase inhibitor has an anti-angiogenic effect at least under our experimental conditions.

In summary, we have shown in the present study that treatment with donepezil attenuated angiogenesis. Stimulation of cholinergic system may be a novel anti-angiogenic therapy.

AUTHOR CONTRIBUTION

Ryohei Miyazaki, Toshihiro Ichiki, Kotaro Takeda and Kenji Sunagawa contributed to the conception and design of the study, and writing of the paper. Ryohei Miyazaki performed the experiments. Jiro Ikeda, Aya Kamiharaguchi, Toru Hashimoto, Eriko Narabayashi and Hirohide Matsuura contributed to the *in vivo* experiments.

ACKNOWLEDGEMENT

We thank the Research Support Center, Kyushu University Graduate School of Medical Sciences for technical support.

FUNDING

This study was supported, in part, by grants-in-aid for Scientific Research from the Ministry of Education, Culture, Sports, Science and Technology of Japan [grant number 19590867]; AstraZeneca Research grant 2007; the Mitsubishi Pharma Research Foundation; the Astellas Foundation for Research on Metabolic Disorders; and the Kimura Memorial Heart Foundation Research Grant for 2009.

REFERENCES

1 Winblad, B., Kilander, L., Eriksson, S., Minthon, L., Batsman, S., Wetterholm, A. L., Jansson-Blixt, C. and Haglund, A. (2006) Donepezil in patients with severe Alzheimer's disease: double-blind, parallel-group, placebo-controlled study. Lancet **367**, 1057–1065
2 Reale, M., Iarlori, C., Gambi, F., Lucci, I., Salvatore, M. and Gambi, D. (2005) Acetylcholinesterase inhibitors effects on oncostatin-M, interleukin-1β and interleukin-6 release from lymphocytes of Alzheimer's disease patients. Exp. Gerontol. **40**, 165–171
3 Rosas-Ballina, M. and Tracey, K. J. (2009) Cholinergic control of inflammation. J. Intern. Med. **265**, 663–679
4 Borovikova, L. V., Ivanova, S., Zhang, M., Yang, H., Botchkina, G. I., Watkins, L. R., Wang, H., Abumrad, N., Eaton, J. W. and Tracey, K. J. (2000) Vagus nerve stimulation attenuates the systemic inflammatory response to endotoxin. Nature **405**, 458–462
5 Wang, H., Liao, H., Ochani, M., Justiniani, M., Lin, X., Yang, L., Al-Abed, Y., Wang, H., Metz, C., Miller, E. J. et al. (2004) Cholinergic agonists inhibit HMGB1 release and improve survival in experimental sepsis. Nat. Med. **10**, 1216–1221
6 de Jonge, W. J., van der Zanden, E. P., The, F. O., Bijlsma, M., van Westerloo, D. J., Bennink, R. J., Berthoud, H. R., Uematsu, S., Akira, S., van den Wijngaard, R. M. and Boeckxstaens, G. E. (2005) Stimulation of the vagus nerve attenuates macrophage activation by activating the Jak2-STAT3 signaling pathway. Nat. Immunol. **6**, 844–851
7 Taqueti, V. R., Mitchell, R. N. and Lichtman, A. H. (2006) Protecting the pump: controlling myocardial inflammatory responses. Annu. Rev. Physiol. **68**, 67–95
8 Hoefer, I. E., van Royen, N., Rectenwald, J. E., Bray, E. J., Abouhamze, Z., Moldawer, L. L., Voskuil, M., Piek, J. J., Buschmann, I. R. and Ozaki, C. K. (2002) Direct evidence for tumor necrosis factor-alpha signaling in arteriogenesis. Circulation. **105**, 1639–1641
9 Carmeliet, P. (2003) Angiogenesis in health and disease. Nat. Med. **9**, 653–660
10 Tateno, K., Minamino, T., Toko, H., Akazawa, H., Shimizu, N., Takeda, S., Kunieda, T., Miyauchi, H., Oyama, T., Matsuura, K. et al. (2006) Critical roles of muscle-secreted angiogenic factors in therapeutic neovascularization. Circ. Res. **98**, 1194–1202
11 Bhat, R. V., Turner, S. L., Marks, M. J. and Collins, A. C. (1990) Selective changes in sensitivity to cholinergic agonists and receptor changes elicited by continuous physostigmine infusion. J. Pharmacol. Exp. Ther. **255**, 187–196
12 Saxena, G., Singh, S. P., Agrawal, R. and Nath, C. (2008) Effect of donepezil and tacrine on oxidative stress in intracerebral streptozotocin-induced model of dementia in mice. Eur. J. Pharmacol. **581**, 283–289
13 Heeschen, C., Jang, J. J., Weis, M., Pathak, A., Kaji, S., Hu, R. S., Tsao, P. S., Johnson, F. L. and Cooke, J. P. (2001) Nicotine stimulates angiogenesis and promotes tumor growth and atherosclerosis. Nat. Med. **7**, 833–839
14 Choi, K. M., Zhu, J., Stoltz, G. J., Vernino, S., Camilleri, M., Szurszewski, J. H., Gibbons, S. J. and Farrugia, G. (2007) Determination of gastric emptying in nonobese diabetic mice. Am. J. Physiol. Gastrointest. Liver Physiol. **293**, G1039–G1045

15 Baschong, W., Suetterlin, R. and Laeng, R. H. (2001) Control of autofluorescence of archival formaldehyde-fixed, paraffin-embedded tissue in confocal laser scanning microscopy (CLSM). J. Histochem. Cytochem. **49**, 1565–1572
16 Imayama, I., Ichiki, T., Inanaga, K., Ohtsubo, H., Fukuyama, K., Ono, H., Hashiguchi, Y. and Sunagawa, K. (2006) Telmisartan downregulates angiotensin II type 1 receptor through activation of peroxisome proliferator-activated receptor γ. Cardiovasc. Res. **72**, 184–190
17 Amano, K., Okigaki, M., Adachi, Y., Fujiyama, S., Mori, Y., Kosaki, A., Iwasaka, T. and Matsubara, H. (2004) Mechanism for IL-1β-mediated neovascularization unmasked by IL-1β knock-out mice. J. Mol. Cell. Cardiol. **36**, 469–480
18 Turner, N. A., Mughal, R. S., Warburton, P., O'Regan, D. J., Ball, S. G. and Porter, K. E. (2007) Mechanism of TNF-α -induced IL-1α, IL-1β and IL-6 expression in human cardiac fibroblasts: effects of statins and thiazolidinediones. Cardiovasc. Res. **76**, 81–90
19 Singh, S., Loke, Y. K. and Furberg, C. D. (2008) Inhaled anticholinergics and risk of major adverse cardiovascular events in patients with chronic obstructive pulmonary disease: a systematic review and meta-analysis. JAMA, J. Am. Med. Assoc. **300**, 1439–1450
20 Tashkin, D. P., Celli, B., Senn, S., Burkhart, D., Kesten, S., Menjoge, S. and Decramer, M. (2008) A 4-year trial of tiotropium in chronic obstructive pulmonary disease. N. Engl. J. Med. **359**, 1543–1554
21 Wessler, I., Kirkpatrick, C. J. and Racke, K. (1999) The cholinergic 'pitfall': acetylcholine, a universal cell molecule in biological systems, including humans. Clin. Exp. Pharmacol. Physiol. **26**, 198–205
22 Hamann, M., Chamoin, M. C., Portalier, P., Bernheim, L., Baroffio, A., Widmer, H., Bader, C. R. and Ternaux, J. P. (1995) Synthesis and release of an acetylcholine-like compound by human myoblasts and myotubes. J. Physiol. **489**, 791–803
23 Pavlov, V. A., Ochani, M., Gallowitsch-Puerta, M., Ochani, K., Huston, J. M., Czura, C. J., Al-Abed, Y. and Tracey, K. J. (2006) Central muscarinic cholinergic regulation of the systemic inflammatory response during endotoxemia. Proc. Natl. Acad. Sci. U.S.A. **103**, 5219–5223
24 Deguchi, J. O., Yamazaki, H., Aikawa, E. and Aikawa, M. (2009) Chronic hypoxia activates the Akt and β-catenin pathways in human macrophages. Arterioscler., Thromb., Vasc. Biol. **29**, 1664–1670
25 Kakinuma, Y., Furihata, M., Akiyama, T., Arikawa, M., Handa, T., Katare, R. G. and Sato, T. (2010) Donepezil, an acetylcholinesterase inhibitor against Alzheimer's dementia, promotes angiogenesis in an ischemic hindlimb model. J. Mol. Cell. Cardiol. **48**, 680–693
26 Kim, J. A., March, K., Chae, H. D., Johnstone, B., Park, S. J., Cook, T., Merfeld-Clauss, S. and Broxmeyer, H. E. (2010) Muscle-derived $Gr1^{dim}CD11b^{+}$ cells enhance neovascularization in an ischemic hind limb mouse model. Blood **116**, 1623–1626
27 Qi, X., Okamoto, Y., Murakawa, T., Wang, F., Oyama, O., Ohkawa, R., Yoshioka, K., Du, W., Sugimoto, N., Yatomi, Y. et al. (2010) Sustained delivery of sphingosine-1-phosphate using poly(lactic-co-glycolic acid)-based microparticles stimulates Akt/ERK-eNOS mediated angiogenesis and vascular maturation restoring blood flow in ischemic limbs of mice. Eur. J. Pharmacol. **634**, 121–131

Received 6 December 2011/26 January 2012; accepted 28 February 2012
Published as Immediate Publication 28 February 2012, doi:10.1042/CS20110633

online data

Clinical Science (2012) **123**, 241–249 (Printed in Great Britain) doi:10.1042/CS20110633

SUPPLEMENTARY ONLINE DATA

Acetylcholinesterase inhibitors attenuate angiogenesis

Ryohei MIYAZAKI*, Toshihiro ICHIKI*†, Toru HASHIMOTO*, Jiro IKEDA*, Aya KAMIHARAGUCHI*, Eriko NARABAYASHI*, Hirohide MATSUURA*, Kotaro TAKEDA*† and Kenji SUNAGAWA*

*Departments of Cardiovascular Medicine, Kyushu University Graduate School of Medical Sciences, Fukuoka, Japan, and †Advanced Therapeutics for Cardiovascular Diseases, Kyushu University Graduate School of Medical Sciences, Fukuoka, Japan

Table S1 Sequences of the primers used in real-time PCR

Angpt 1 and 2, angiopoietin 1 and 2; PlGF, placental growth factor.

	Sequence (5′→3′)	
Gene	Forward	Reverse
TNFα	AAGCCTGTAGCCCACGTCGTA	GGCACCACTAGTTGGTTGTCTTTG
IL-1β	GCAACTGTTCCTGAACTCAACT	ATCTTTTGGGGTCCGTCAACT
IL-6	CCACTTCACAAGTCGGAGGCTTA	GCAAGTGCATCATCGTTGTTCATAC
VEGF	GCACATAGGAGAGATGAGCTTCC	CTCCGCTCTGAACAAGGCT
Angpt1	CCGAGCCTACTCACAGTACGACAG	AAATCGGCACCGTGTAAGATCAA
Angpt2	GGACAGTCATCCAACACCGAGA	CAAACTCATTGCCCAGCCAGTA
PDGF	CAAAGGCAAGCACCGAAAGTTTA	CCGAATCAGGCATCGAGACA
bFGF	GTGCCAACCGGTACCTTGCTA	TCAGTGCCACATACCAACTGGAG
PlGF	CCTGTCTGCTGGGAACAACTCA	CACCTCATCAGGGTATTCATCCAAG
CD3ε	CACTCTGGGCTTGCTGATGG	TCATAGTCTGGGTTGGGAACAGG
F4/80	GAGATTGTGGAAGCATCCGAGAC	GATGACTGTACCCACATGGCTGA
β-Actin	GGCTGTATTCCCCTCCATCG	CCAGTTGGTAACAATGCCATG

Table S2 HR, BP and body weight in the experimental groups

Results are means ± S.E.M. *$P < 0.05$ compared with control.

Group	HR (beats/min)	SBP (mmHg)	Body weight (g)
Control	555 ± 34	101 ± 10	24.8 ± 0.8
Donepezil	452 ± 31*	97 ± 6	23.3 ± 0.3
Physostigmine	501 ± 20	100 ± 2	23.2 ± 0.7
Nicotine	522 ± 56	101 ± 17	24.3 ± 1.9
Betahnechol	472 ± 47	95 ± 8	23.8 ± 1.9

Table S3 HR, BP and body weight in the experimental groups treated with donepezil with or without IL-1β

Results are means ± S.E.M.

Group	HR (beats/min)	SBP (mmHg)	Body weight (g)
Control + PBS	531 ± 21	104 ± 6	24.1 ± 0.5
Donepezil + PBS	490 ± 26	100 ± 4	23.7 ± 1.7
Donepezil + IL-1β	501 ± 8	105 ± 3	23.6 ± 0.6

Received 6 December 2011/26 January 2012; accepted 28 February 2012
Published as Immediate Publication 28 February 2012, doi:10.1042/CS20110633

Correspondence: Professor Toshihiro Ichiki (email ichiki@cardiol.med.kyushu-u.ac.jp).

INTERNAL MEDICINE

□ ORIGINAL ARTICLE □

Usefulness of Non-contact Mapping for Radiofrequency Catheter Ablation of Inappropriate Sinus Tachycardia: New Procedural Strategy and Long-term Clinical Outcome

Masao Takemoto[1], Yasushi Mukai[1], Shujiro Inoue[1], Tetsuya Matoba[1], Mari Nishizaka[1], Tomomi Ide[1], Akiko Chishaki[2] and Kenji Sunagawa[1]

Abstract

Objectives The present study evaluated the clinical benefits of a new therapeutic method of radiofrequency catheter ablation (RFCA) using an EnSite system for inappropriate sinus tachycardia (IST).

Materials and Methods Six patients with debilitating IST underwent RFCA using EnSite. Using the beta-adrenergic blocker and agonist, the heart rate was controlled between 70 to 150 bpm before and after the RFCA. The areas of the breakout sites (BOSs) were clearly distinguished between those from the normal P-wave zones during rates of less than 100 bpm and those from more upper rate sites during rates of more than 100 bpm using the EnSite system, in accordance with the appearance of tall P-waves (tall P-wave zone) in the IST patients. This was selected as the target for ablation.

Results After the RFCA, the BOSs observed during heart rates of more than 100 bpm moved completely from the tall P-wave zone to the normal P-wave zone in the IST patients. The total number of heart beats and average heart beat on the 24-h Holter monitoring decreased statistically from that before the RFCA to that after, and no adverse heart rate responses was observed after the RFCA. Before the RFCA, the brain natriuretic peptide was elevated, New York Heart Association functional class was worse, and there was an impaired exercise tolerance observed with exercise electrocardiogram testing. The RFCA for the IST significantly improved those parameters.

Conclusion This new therapeutic method for IST using EnSite is effective and produces clinical benefits.

Key words: inappropriate sinus tachycardia, non-contact mapping, catheter ablation

(Intern Med 51: 357-362, 2012)
(DOI: 10.2169/internalmedicine.51.5882)

Introduction

Inappropriate sinus tachycardia (IST) is an uncommon clinical syndrome that is characterized by an elevated resting heart rate or disproportionate increase in the rate with minimal exertion (1). This condition is predominantly encountered in women and common symptoms include palpitations, presyncope/syncope, chest pain, dizziness, shortness of breath, anxiety and depression (2). Radiofrequency (RF) catheter ablation (RFCA) is an acceptable treatment modality for drug refractory IST, and several procedural strategies for sinus node (SN) modification have been described (1-3). Here we report our new observations using a non-contact mapping system, EnSite (St. Jude Medical, Minnetonka, MN, USA) in patients with drug refractory IST.

Materials and Methods

Study population and laboratory analysis

From 2006 to 2009, 6 consecutive patients (3 males and 3 females with a mean age of 43 ± 3 years old) with drug refractory (including beta-blockers, calcium-channel blockers,

[1]Department of Cardiovascular Medicine, Kyushu University Hospital, Japan and [2]Department of Health Sciences, Kyushu University Graduate School of Medical Sciences, Japan
Received for publication May 24, 2011; Accepted for publication November 2, 2011
Correspondence to Dr. Masao Takemoto, matakemo@cardiol.med.kyushu-u.ac.jp

and digitalis) IST underwent RFCA in our hospital. All patients had their history recorded, and underwent a physical examination, laboratory analysis, chest X-ray, 12-lead electrocardiogram, 24-h Holter monitoring, M-mode, two-dimensional and Doppler echocardiograms, and exercise electrocardiogram testing on admission or within at least 1 month before the admission, and 2 or 3 days after the RFCA. These examinations yielded no evidence of clinically overt structural heart disease, including coronary artery disease, valvular heart disease, congenital heart disease, LV hypertrophy, or RV abnormalities in any of the patients. The serum brain natriuretic peptide (BNP) concentration and New York Heart Association (NYHA) functional class were evaluated on admission and 6 to 12 months after the RFCA. The mean follow-up period was 29 ± 2 months.

Definition of IST

IST was defined as: 1) a P-wave axis and morphology during the tachycardia similar to that during sinus rhythm, and tall P-waves during the tachycardia which were at least 2-fold taller than those during sinus rhythm, especially in leads II, III, and aVF, 2) a heart rate of greater than 100 beats per minute (bpm) at rest or with minimal exertion, 3) exclusion of any secondary causes of tachycardia, 4) 24-h Holter monitoring demonstrating a mean heart rate of greater than 90 bpm, and 5) a heart rate of greater than 130 bpm within the first 90 seconds of a standard Bruce protocol on the treadmill test (1, 4, 5).

Mapping and catheter ablation procedure

All procedures were performed after written informed consent was obtained. The patients were studied in the fasting state without sedation. Antiarrhythmic drugs and beta-blockers were discontinued for at least five half-lives before the procedure. Under local anesthesia, two multipolar electrode catheters (St. Jude Medical, Tokyo, Japan) were placed percutaneously in the coronary sinus and high right atrium (RA), and His-bundle and right ventricle, respectively. A multielectrode array catheter utilizing EnSite 3.2 or EnSite 6.0J was positioned in the RA approximately at the level of the superior vena cava and RA junction with the distal end oriented superiorly using a guidewire (Fig. 1A, B). Thus, the distance between EnSite array and sinus node was less than 4 cm. A 7-F deflectable quadripolar ablation catheter, Ablaze or Fantasista (Japan Lifeline Co., Ltd., Tokyo, Japan) with a 4-mm-tip electrode was also introduced percutaneously into the RA, and the baseline RA geometry was acquired. An electrophysiological study (EPS) was performed before and after RFCA to verify the mechanism of arrhythmia and to exclude the coexistence of other arrhythmias.

Using an intravenous administration of the beta-adrenergic blocker, landiolol (5 to 40 μg/kg/min) and agonist, isoproterenol (ISP) (2 to 5 μg intravenous administration), the heart rate was controlled between 70 to 150 bpm before and after the RFCA. Then, the origins which indicated the SN during sinus rhythm and IST were defined as the earliest sites showing a single spot on the isopotential map and a QS pattern in the noncontact unipolar electrograms, as previously described (6). The breakout sites (BOSs) during sinus rhythm and IST were also defined as the earliest sites that showed an rS pattern with a sudden increase in the peak negative potential of the noncontact unipolar electrogram. These origins and BOSs were tagged for each heart rate on the RA geometry (Fig. 1C-H, 2A-J)). In all patients, compared to that during heart rates of less than 100 bpm with normal P-waves (normal P-wave zone), the BOSs steadily moved to more upper rate sites during heart rates of more than 100 bpm in accordance with the appearance of tall P-waves (tall P-wave zone) (Fig. 1C-J, 2A-J). The SN and BOSs within normal P-wave zones and tall P-wave zones could easily and clearly be separated by this method. The RF energy was delivered to the tall P-wave zones, and not to the SN or normal P-wave zones, for 30 to 60 seconds with a preset temperature of 50℃ and power limit of 30W. In 4 of 6 patients, repetitive atrial response was observed. The average distance between SN and ablation site was 12.7 ± 0.7 mm. A successful RFCA was defined as that when the BOSs observed during heart rates of more than 100 bpm (100 to 150 bpm) moved completely from the tall P-wave zone to the normal P-wave zone (Fig. 2C, D, E, H-J) with and without the intravenous administration of isoproterenol in accordance with the abolishment of the tall P-waves on the 12-lead electrocardiogram during the RF energy delivery (arrows in Fig. 1K). All 12-lead electrocardiograms and the bipolar intracardiac electrograms (filtered at 30 to 400 Hz) were recorded and stored using a 96-channnel acquisition system (CardioLabEP, Prucka Engineering Inc., Houston, TX, USA). During the procedure, intravenous heparin was given as a 5,000-unit bolus dose.

Statistical analysis

The numerical results are expressed in the text as the mean ± standard deviation. Paired data were compared by a Student's *t* test. A value of $p<0.05$ was considered to indicate statistical significance.

Results

Patient characteristics

Although patients primarily women in this syndrome, 50% were male in this study. An RFCA procedure for IST was performed in 6 patients. Procedural success was achieved in all 6 (100%) of the patients. No patients suffered from any procedure-related complications including SN dysfunction (sick sinus syndrome), cardiac tamponade, diaphragmatic paralysis, or superior vena cava syndrome. During 1-year follow-up, no recurrence of IST was observed in any of the patients. However, in 1 of the 6 patients the IST recurred and that patient underwent a repeat RFCA with a successful result a year and a half after the first RFCA.

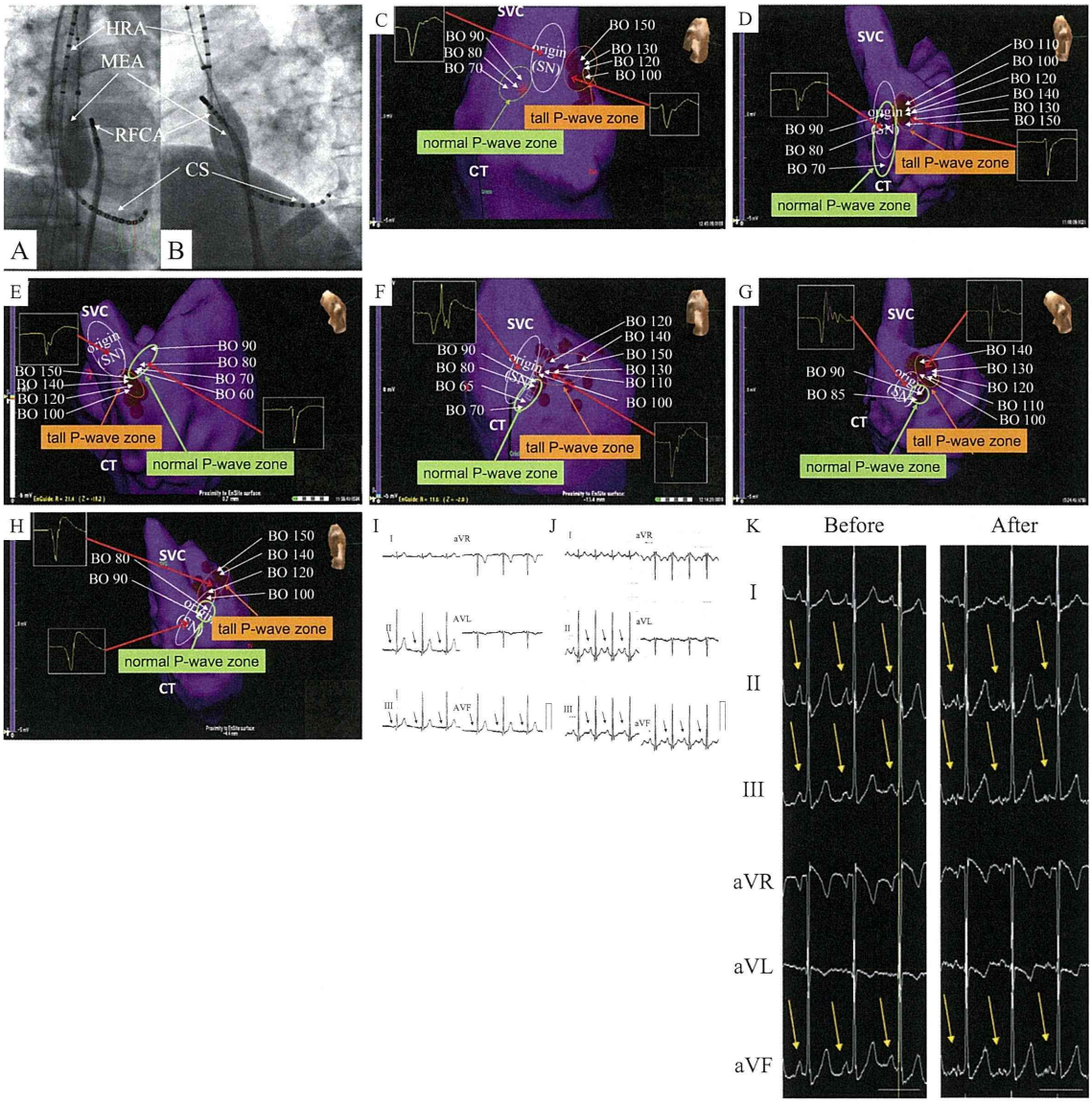

Figure 1. **Fluoroscopic images in the right (RAO; panel A) and left (LAO; panel B) anterior oblique views showing the location of the multipolar electrode catheters, multielectrode array (MEA) catheter, and radiofrequency ablation (RFCA) catheter placed in the high right atrium (HRA), coronary sinus (CS), and right atrium (RA) approximately at the level of the superior vena cava, respectively. The EnSite images of the RA in the RAO view of 6 cases (panel C-H) show the origin which indicates the location of the sinus node (SN) and breakout sites (BOSs) for each heart rate determined by the EnSite. The SN and BOSs, and normal P-wave zone and tall P-wave zone could easily and clearly be separated by the EnSite system. Compared to that for heart rates of less than 100 bpm associated with normal P-waves (arrows in panels I and J), the tall P-waves (arrows in panels J and K) were determined in the electrocardiogram, especially in leads II, III, aVF at heart rates of more than 100 bpm. Crista indicates the crista terminalis. SVC indicates superior vena cava. The bars in panel I and J indicate 1 mV. The bars in panel F indicate 400 ms.**

24-h Holter monitoring (Table 1)

The total number of heart beats and average heart beat statistically differed between that before and that after the RFCA ($p<0.01$) (Table 1). Although the heart rate was greater than 100 bpm at rest or with minimal exertion before the RFCA (Fig. 3A), an adverse heart rate response was not observed after the RFCA (Fig. 3B).

Serum BNP concentration and NYHA functional class

The serum BNP concentration and NYHA functional class were evaluated in all patients on admission and 6 to 12 months after the RFCA. The serum BNP was elevated before the RFCA. However, it significantly decreased 6 to 12 months after the RFCA ($p<0.05$) (Fig. 4A). The NYHA functional class was demonstrated to be significantly worse

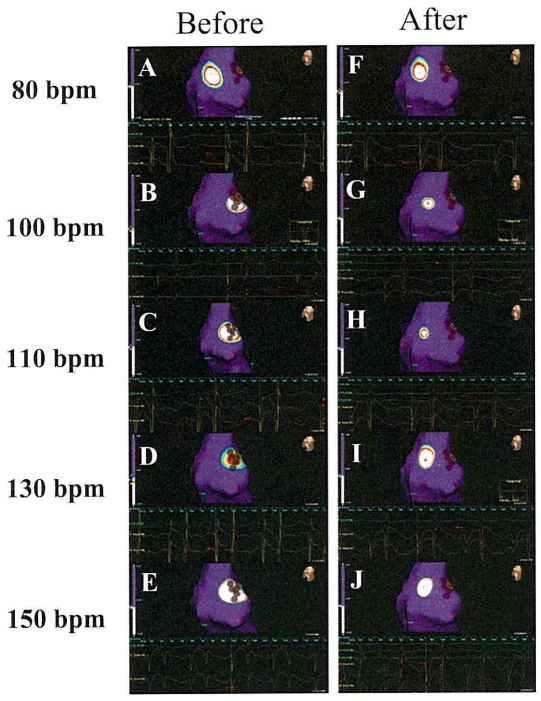

Figure 2. **EnSite images of the right atrium in the right anterior oblique view. Before the radiofrequency catheter ablation (RFCA), compared to that for heart rates of less than 100 bpm associated with normal P-waves (normal P-wave zone), the breakout sites (BOSs) steadily moved to more upper sites during heart rates of more than 100 bpm associated with the appearance of tall P-waves (tall P-wave zone) (A-E). On the other hand, after the RFCA in the tall P-wave zone, the BOSs during heart rates of more than 100 bpm (100 to 150 bpm) moved completely from the tall P-wave zone to the normal P-wave zone with and without the intravenous administration of isoproterenol (F-J). The black lines on the geometry in panels A-J indicate the crista terminalis. RAA indicates right atrial appendage. The breakout sites (BOSs) during sinus rhythm and IST were usually defined as the earliest sites that showed an rS pattern with a sudden increase in the peak negative potential of the noncontact unipolar electrogram. However, QS patterns in the tracking virtual are seen in these figures. Since the origin is located in the epicardium or deep myocardium, the BOS was sometimes recoded as a QS pattern[15] in this present case. There is a possibility that the origin may be located adjacent to the BOS in this case.**

before the RFCA (Fig. 4B). The RFCA significantly improved the NYHA functional class as compared to that before the intervention ($p<0.01$).

Exercise electrocardiogram testing (Table 1)

One of the 6 patients could not perform an exercise electrocardiogram test due to a gait disturbance caused by necrosis of the head of the femur. Compared to that before the RFCA, the resting heart rate significantly decreased after the RFCA ($p<0.05$). The time to achieve a heart rate of 130 bpm took significantly longer after the RFCA than before ($p<0.01$). Moreover, the RFCA significantly improved the exercise tolerance of the IST-patients ($p<0.05$).

Response to beta-adrenergic receptor stimulators (Table 1)

Before the RFCA, a low dose of ISP could steadily increase the patients' heart rate to 150 bpm. However, compared to that before the RFCA, a high dose of ISP was needed to increase the heart rate to 150 bpm ($p<0.01$) after the RFCA.

Patient symptoms and medications (Table 2)

On admission, all patients had IST-associated symptoms including palpitations (100%), general fatigue (83%), depression (67%) and fainting (33%). All patients had been taking antiarrhythmic agents before admission, such as beta-blockers (100%), calcium channel antagonists (33%) and digitalis (17%). However, those agents were not sufficiently effective in eliminating the IST-associated tachycardia and symptoms. All of the patients with a successful procedure reported the absence of any IST-associated tachycardia or symptoms after the RFCA. In 4 of the 6 patients it was possible to discontinue those antiarrhythmic agents. Two of the 6 patients continued to receive the beta-blockers for their hypertension.

Discussion

Major findings and clinical implications

The major findings of this study are as follows: 1) in a short time EnSite could steadily and clearly separate the SN, normal P-wave zone, and tall P-wave zone which was the targeted site of the RFCA (Fig. 1C-H, 2A-J), 2) the RFCA could easily and efficaciously treat the IST without any complications, and 3) all patients were free from any further IST-associated tachycardia (Fig. 3A, B) or symptoms (Table 2) in accordance with a decrease in their heart rate (Table 1), and experienced a dramatic improvement in the inappropriate increase in their heart rate with minimal exertion (Table 1), serum BNP level (Fig. 4A), NYHA functional class (Fig. 4B), and exercise tolerance (Table 1). Some previous studies demonstrated that the recurrence rate was 20 to 50% and some patients underwent a pacemaker implantation (1, 3, 7-9). However, with this method, the recurrence rate was only 1 out of 6 patients (17%) during a mean follow-up period of 29 ± 2 months. The characteristic point of this method which differs from that of the previous studies is that the target site of the RFCA was the BOSs in the tall P-wave zone, and not the SN. Thus, the RF energy could safely and easily be delivered at the target sites (BOSs) without any complications. As a result, this method could achieve an acceptable long-term clinical outcome. This method should be a new safe and effective procedural strategy for IST.

Table 1. Parameters before and after Radiofrequency Catheter Ablation

	Before	After
24-h Holter Monitoring Analysis (n=6)		
total HB (x10^3 beats/day)	134 ± 2	113 ± 2**
average HB (beats/minute)	93 ± 1	79 ± 1**
Exercise Eelectrocardiogram Testing Analysis (n=5)		
Resting HR (beats/minute)	108 ± 2	95 ± 2 *
Time-HR130 (seconds)	76 ± 5	212 ± 5**
Exercise tolerance (Mets)	6.8 ± 0.4	9.3 ± 0.6*
Response to Beta-adrenergic Receptor Stimulator (n=6)		
ISP dose achieved HR150 bpm (μg)	2.8 ± 0.2	4.8 ± 0.3**

**p<0.01, *p<0.05 versus before RFCA, HB = heart beats; HR = heart rate; Time-HR130 = time achieved 130 bpm of the heart rate; ISP = isoproterenol.

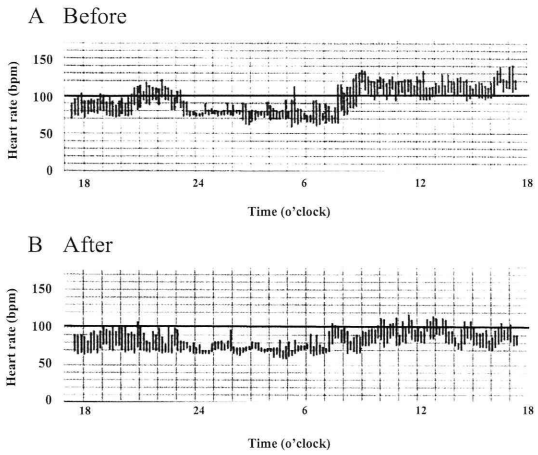

Figure 3. The 24-h Holter monitoring before and after the radiofrequency catheter ablation (RFCA). The heart rate was greater than 100 bpm at rest or with minimal exertion before the RFCA (A). However, that adverse heart rate response was not observed after the RFCA (B).

Mechanism of IST

Although the mechanism(s) of IST has not been completely elucidated, several potential mechanisms have been raised include the following: 1) autonomic dysfunction including an increased sympathetic tone and/or receptor sensitivity, blunted parasympathetic tone, or sympathovagal imbalance (2, 10), 2) abnormal automaticity of the SN (2, 11), 3) an atrial tachycardia focus near the SN (2), and 4) dysautonomia involving the anterior right ganglionated plexi (ARGP) (12, 13).

In this method, the target of the RFCA sites was the BOSs in the tall P-wave zone, and not the SN, indicating that abnormal automaticity of the SN may not be the potential mechanism of IST (14). The distinction between a focal atrial tachycardia and IST is often difficult to make. Occasionally, this distinction can be made clinically in that atrial tachycardia may not be related to activity with an unpredictable onset of the tachycardia at rest or with minimal exertion. Moreover, the BOSs of the tachycardia shifts for each different heart rate. This point may differentiate IST from focal atrial tachycardia.

It has been reported that epinephrine injected into the ARGP, which is located in the fat pad at the base of the right pulmonary veins adjacent to the caudal end of the SN, induces IST, and ablation of the ARGP eliminated the IST without damaging the SN (12, 13). Since the ablation sites were near the SN in this study, it may be possible that the ARGP may have been ablated. However, we could not sufficiently explain why the BOSs moved from the tall P-wave zone to the normal P-wave zone. Further studies may be needed to explain this.

We assumed that two types of autonomic regulation may exist, because there are two types of BOSs, those associated with a tall P-wave zone and those with a normal P-wave zone. Since the response to beta-adrenergic receptor stimulators differed before and after the RFCA (Table 1), one type of autonomic regulation may be an increased sympathetic tone and/or receptor sensitivity. Thus, the ablation of these abnormal autonomic regulation sites may abolish the IST-associated tachycardia, and improve the response to beta-adrenergic receptor stimulators. As a result, the BOSs shifted from the tall-P wave zone, possibly autonomic regulation sites, to the normal P-wave zone, possibly normal autonomic regulation sites.

Limitation of this study

The patient number of this study is comparably small. This arrhythmia involves several mechanisms such as primary sinus node abnormality, depressed efferent cardiovagal reflex and beta-adrenergic hypersensitivity (11). Not all of the patients with this arrhythmia may show a similar response to landiolol or isoproterenol. The similar trend in the response might occur only in a small subgroup of patients with this arrhythmia.

Conclusion

Finally, this new therapeutic method for ablating IST using the EnSite system was effective and safe. Although IST is an uncommon clinical syndrome, it has disabling symptoms. Thus, physicians should be aware of this condition when examining a patient with a tachycardia characterized by an elevated resting heart rate or a disproportionate increase in the heart rate with minimal exertion. Since IST is often drug-refractory, RFCA utilizing EnSite may be considered as the first choice of therapy in such patients.

The authors state that they have no Conflict of Interest (COI).

Acknowledgement

We thank Ryoko Hayashi, Kou Adachi, Keiji Kobayashi, and Noriko Nakajima for their technical assistance with the electrophysiological studies in the cardiac catheterization laboratory, and John Martin for his linguistic assistance with this paper.